HHS Public Access

Author manuscript

Toxicol Sci. Author manuscript; available in PMC 2024 January 31.

Published in final edited form as:

Toxicol Sci. 2023 January 31; 191(1): 61–78. doi:10.1093/toxsci/kfac113.

Aerosol physicochemical determinants of carbon black and ozone inhalation co-exposure induced pulmonary toxicity

Nairrita Majumder[#,1,2], **Vamsi Kodali**[#,1,2,3], **Murugesan Velayutham**[1,2,4], **Travis Goldsmith**[1,2], **Jessica Amedro**[1], **Valery V. Khramtsov**[4], **Aaron Erdely**[1,2,3], **Timothy R. Nurkiewicz**[1,2,3], **Jack R. Harkema**[5], **Eric E. Kelley**[1,2,3], **Salik Hussain**[*,1,2,3]

[1]Department of Physiology and Pharmacology, School of Medicine, West Virginia University, Morgantown, WV 26506.

[2]Center for Inhalation Toxicology (*iTOX*), School of Medicine, West Virginia University, Morgantown, WV 26506.

[3]Health Effects Laboratory Division, National Institute for Occupational Safety and Health (NIOSH), Morgantown, WV 26508

[4]Department of Biochemistry and Molecular Medicine, School of Medicine, West Virginia University, Morgantown, WV 26506.

[5]Department of Pathobiology and Diagnostic Investigation, College of Veterinary Medicine, Michigan State University, East Lansing, MI 48824

Abstract

Air pollution accounts for more than 7 million premature deaths worldwide. Using ultrafine carbon black (CB) and ozone (O_3) as a model for an environmental co-exposure scenario, the dose response relationships in acute pulmonary injury and inflammation were determined by generating, characterizing, and comparing stable concentrations of CB aerosols (2.5, 5.0, 10.0 mg/m^3), O_3 (0.5, 1.0, 2.0 ppm) with mixture CB+O_3 (2.5 + 0.5, 5.0 + 1.0, 10.0 + 2.0). C57BL6 male mice were exposed for 3 hours by whole body inhalation and acute toxicity determined after 24h. CB itself did not cause any alteration, however, a dose response in pulmonary injury/inflammation was observed with O_3 and CB+O_3. This increase in response with mixtures was not dependent on the uptake but due to enhanced reactivity of the particles. Benchmark dose modeling showed several-fold increase in potency with CB+O_3 compared to CB or O_3 alone. Principal component analysis provided insight into response relationships between various doses and treatments. There was a significant correlation in lung responses with charge-based size

[*]**Corresponding Author**: Salik Hussain DVM, PhD, Department of Physiology and Pharmacology, Center for Inhalation Toxicology (iTOX), School of Medicine, West Virginia University, Morgantown, 26506, WV 304-293-8047 salik.hussain@hsc.wvu.edu.
[#]Nairrita Majumder and Vamsi Kodali contributed equally

Declaration of competing interest

The authors declare that they have no known competing financial interests or personal relationships that could have appeared to influence the work reported in this paper.

Disclaimer

The findings and conclusions in this report are those of the author(s) and do not necessarily represent the official position of the National Institutes of Health and National Institute for Occupational Safety and Health, Centers for Disease Control and Prevention. Mention of brand name does not constitute product endorsement.

distribution, total/alveolar deposition, oxidant generation and antioxidant depletion potential. Lung tissue gene/protein response demonstrated distinct patterns that are better predicted by either particle dose/aerosol responses (IL-1β, KC, TGF-β) particle reactivity (TSLP, IL13, IL-6). Hierarchical clustering showed a distinct signature with high dose and a similarity in mRNA expression pattern of low and medium doses of CB+O_3. In conclusion, we demonstrate that the biological outcomes from CB+O_3 co-exposure are significantly greater than individual exposures over a range of aerosol concentrations and aerosol characteristics can predict biological outcome.

Graphical Abstract

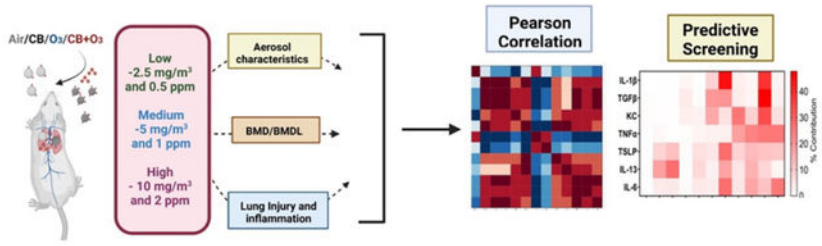

Keywords

Ozone; Ultrafine Carbon Black; Physicochemical Properties; Inhalation; Co-exposure; Inflammation

Introduction:

Inhalation co-exposure to ultrafine particulate and gaseous components of air pollution represent more realistic exposure scenario compared to individual particulate or gaseous exposures. The World Health Organization (WHO) attribute air pollution to be associated with approximately 7 million premature deaths per year making it one of the top five causes of mortality (Organization 2016). A significant increase in morbidity, hospitalizations and economic losses (lost workdays) are also associated with air pollution (Birnbaum et al. 2020). In the past year, approximately 160 million individuals in the United States breathe air exceeding federal air quality standards (GBDCRD 2017; GBDRFC 2016). These levels, although lower than many more polluted areas of the world, are still effective in exacerbating cardio-respiratory and other systemic conditions in vulnerable populations (GBDCRD 2017; GBDRFC 2016). Both short- and long-term exposure to particulate matter significantly increase mortality, morbidity, and hospitalization rates (Anenberg et al. 2014; Apte et al. 2015). Over the last decade, WHO's Air Pollution Health Risk Assessment (AP-HRA) and a significant body of literature have positively associated the major pollutants like ozone (O_3) and particulate matter to cardiopulmonary, systemic, reproductive, as well as cognitive disorders (Campen et al. 2009; Cleary et al. 2018; Ghosh et al. 2021; Shehab and Pope 2019).

Epidemiological data suggests a positive association between co-exposure to particulate matter and gases to pulmonary complication related hospitalization rates (Rhee 2018). A growing body of evidence suggest interactive effects of exposure to different types

of particulates and gases including O_3, NO_2, and volatile organic compounds (Mauderly and Samet 2009). Co-exposure to particulate matter and O_3 has already been linked to aggravated cardiovascular outcomes, exacerbated lung injury in pre-existing cardiovascular disease and increased airway and systemic inflammation in elderly subjects (Hamade et al. 2010; Hamade et al. 2008; Holz et al. 2018; Wagner et al. 2014; Wong et al. 2018).

We recently described an ultrafine carbon black (CB) and O_3 inhalation co-exposure model to more accurately replicate particle and gases mixed exposures (Hathaway et al. 2021; Majumder et al. 2021a; Majumder et al. 2021b). Ground level O_3 is one of the most reactive components of air pollution and is classified as a criteria pollutant by the United States Environmental Protection Agency (US EPA). Epidemiological and clinical studies confirm a strong association between short term acute exposure to O_3 and exacerbation of pre-existing lung conditions in vulnerable population (Farhat et al. 2013; Fauroux et al. 2000; Yang et al. 2003). The EPA estimate a linear relationship between O_3 and global warming, anticipating an approximately 14% increase in O_3 associated mortality level across the globe by 2030 (Wilson et al. 2017). CB is a significant occupational and environmental health hazard, with a wide range of application as a reinforcing agent in rubber, paints, and in leather industries (Pirela et al. 2017; Rattanasom et al. 2007; Singh et al. 2022). Occupational exposure to CB is associated with inflammation and decline in lung function (Harber et al. 2003; Zhang et al. 2014).

Previous studies on particulate matter as well as nanoparticles clearly underpin the role of physicochemical characteristics in dictating the biological activity of the particulates (Braakhuis et al. 2014; Hussain et al. 2009; Hussain et al. 2010; Nurkiewicz et al. 2008; Shin et al. 2015). While, this phenomenon is well known for the ultrafine/nanoparticles, the relative contribution/association of different aerosol characteristics with biological activity in case of ultrafine CB and O_3 mixed exposure is not known. Further, more computational approaches to predict biological activity based on aerosol characteristics are clearly needed to help hazard identification/risk assessment of an ever-growing number of aerosols. The purpose of this study was to elaborate the relationship between different aerosol physicochemical characteristics, oxidative properties, and uptake with pulmonary injury and inflammation using three different exposure levels. Apart from the multivariate analysis, we also used predictive screening (boot strap forest) to determine the relative contribution of these characteristics in co-exposure induced inflammatory protein secretions. We hypothesized that the contribution of differential macrophage uptake and alteration in physicochemical characteristics play important role in co-exposure induced increased biological activity.

2. Materials and Methods:

Exposure System, Aerosol Generation, and Characterization:

Whole-body inhalation exposures were conducted at various concentrations of CB aerosols (2.5, 5.0, 10.0 mg/m^3), O_3 gas (0.5, 1.0, 2.0 PPM) or mixtures of the two toxicants (2.5 CB / 0.5 O_3, 5.0 CB / 1.0 O_3, 10.0 CB / 2.0 O_3). The exposure system has been detailed previously (Hathaway et al. 2021; Majumder et al. 2021a; Majumder et al. 2021b). Briefly, bulk CB material (Printex 90®, provided as a gift from Evonik, Frankfurt, Germany) was

aerosolized with a high-pressure acoustical generator (HPAG, IEStechno, Morgantown, WV) then further deagglomerated with a venturi pump (JS-60M, Vaccon, Medway MA) attached to the output of the generator. A light scattering device (pDr-1500, Thermo Environmental Instruments Inc, Franklin, MA) was used to estimate the mass concentration of the aerosol. O_3 gas was generated (HTU500AC, Ozone Solutions, Hull, IA) and mixed with the CB aerosol and fed into a stainless-steel exposure chamber (Cube 150, IEStechno, Morgantown, WV). Chamber O_3 levels were measured with a calibrated monitor (Model 202, 2B Technologies, Inc., Boulder, CO). O_3 monitor calibration was independently verified using calorimetric O_3 gas detector tubes (Sensidyne® LP, St Petersburgh FL). Mice were individually housed in stainless-steel mesh cages within the chamber and the temperature (20–22 °C) and humidity (50–70%) were monitored and maintained within accepted animal comfort levels during exposures. Gravimetric measurements were conducted with 37 mm PTFE filters to report exposure mass concentrations and to continually calibrate the pDr-1500. The CB and O_3 levels were kept at constant, user-defined levels during exposures with automated feedback loops. Particle size distributions of the CB aerosol were periodically sampled from the exposure chamber with: 1) an electrical low-pressure impactor (ELPI+, Dakati, Tempera, Finland), 2) an aerosol particle sizer (APS 3321, TSI Inc Shoreview, MN), and 3) a scanning mobility particle sizer (SMPS 3938, TSI Inc. Shoreview, MN). Elemental composition at CB and CB+O_3 particle surfaces was analyzed using X-Ray Photo Electron Spectroscopy (XPS) technique using Physical electronics PHI 5000 Versa Probe XPS/UPS.

Lung Histopathology:

The non-lavaged lungs were fixed by tracheal instillation of 10% neutral buffered formalin. Fixed tissue were processed for light microscopy. Random transverse tissue blocks from the left lung lobes were paraffin embedded, sectioned at a thickness of 5 microns and stained with hematoxylin and eosin (H&E). Severity of exposure-related lung lesions were semi-quantitively scored via light microscopic examination, by a board-certified veterinary pathologist (JRH) in a blinded manner (no knowledge of individual exposure conditions). Criteria-based scores for specific airway (bronchioles/alveolar duct) lesions (inflammation, epithelial necrosis/exfoliation/loss, monocyte/macrophage hyperplasia) were 0, no histopathology; 1, minimal, < 10% of airway tissue affected; 2, mild, 10% < 25% airway tissue affected; 3, moderate, 25% < 50% airway tissue affected; 4, marked, 50% < 75% airway tissue affected; 5, severe, 75% - 100% airway tissue affected.

Electron Paramagnetic Resonance (EPR) Spectroscopic Studies:

EPR spin probe CMH (1-hydroxy-3-carboxymethyl-2,2,5,5-tetramethyl-pyrrolidine; Enzo Life Sciences, Farmingdale, New York) was used to quantify the oxidant potential of CB particles collected from exposure chamber in the presence or absence of O_3. The particles (CB, CB+O_3 – 10.0 mg/m^3 + 2.0 ppm, 5.0 mg/m^3 + 1.0 ppm, and 2.5 mg/m^3 + 0.25 ppm) were suspended at a concentration of 50 μg/mL in a cell culture grade sterile PBS (treated with Chelex 100), followed by incubation for 30 mins at 37 °C with 200 μM CMH. The serum samples were collected after exposure to CB particles with and without O_3 at different concentrations and were incubated with 200 μM CMH spin probe for 30 mins at 37 °C. The samples were flash frozen in liquid nitrogen and stored at −80°C for further quantification.

Bruker EMXnano spectrometer (Bruker BioSciences, Billerica, MA, USA) was used to measure the EPR active CM• radical which was formed due to the oxidation of CMH by the oxidative species on the surface of the CB particles.

At the time of EPR measurements, liquid samples were thawed and loaded (50 μL) into glass capillary tubes that were sealed on one end using Critoseal clay and placed inside a 4 mm (O.D.) EPR quartz tube. The quartz tube was positioned inside the resonator/cavity and EPR spectra were recorded at room temperature. The following EPR instrument settings were used: microwave frequency, 9.615 GHz; sweep width, 100 G; microwave power, 20 mW; modulation amplitude, 1 G; modulation frequency, 100 kHz; receiver gain, 50 dB; time constant, 10.24 ms; conversion time, 30 ms, sweep time, 30 s; number of scans, 1.

Ferric Reducing Ability of Serum (FRAS) Assay:

The FRAS assay solution was prepared as described previously (Majumder et al. 2021a). FRAS assay was used to screen the acellular oxidant potential of the particles by quantifying the particulate capacity for antioxidant depletion. Serum is a rich source of various types of antioxidants. The antioxidant depletion potential of CB and CB+O_3 particles was measured by reacting human serum (Sigma Aldrich, St. Louis, MO) with particles (CB, CB+O_3 – 10.0 mg/m^3 + 2.0 ppm, 5.0 mg/m^3 + 1.0 ppm and 2.5 mg/m^3 + 0.5 ppm) at a concentration of 5.0 mg/mL, followed by sonication and incubation in a shaker at 450 RPM at 37 °C for 3 hours. The particles were separated after the incubation by centrifugation at 14,000 g for 30 mins. This was followed by addition of 50 μL of serum to 1 mL of FRAS solution, as described previously (Majumder et al. 2021b). The formation of blue color in the solution due to ferrous-tripyridyltriazine complex was measured at 586 nm wavelength in Spectramax iD5 plate reader and reported as percentage change from control human serum. The reduction in the antioxidant capacity of serum was quantified and reported as percentage change with respect to control human serum.

Inhalation Exposures:

All animal procedures were approved by the WVU Institutional Animal Care and Use Committee (IACUC). C56BL/6J male mice (8 weeks old) were purchased from Jackson Laboratory (Bar Harbor, ME) and acclimated at AAALAC accredited animal facility at the West Virginia University Health Sciences Center. WVU is. All animals were maintained in a room with a 12-hour light/dark cycle and provided chow and water *ad libitum*. Mice were randomly divided and exposed to filtered air, three different doses of either CB (10.0 mg/m^3, 5.0 mg/m^3 and 2.5 mg/m^3, or O_3 (2.0 ppm, 1.0 ppm and 0.5 ppm and mixture (CB+O_3) (10.0 mg/m^3 + 2.0 ppm, 5.0 mg/m^3 + 1.0 ppm and 2.5 mg/m^3 + 0.5 ppm) for three hours. These concentrations were referred to as low, medium and high as presented in Table 1. Animals were euthanized 24 hours post exposure by intraperitoneal injection of Fatal Plus® (Pentobarbital Sodium, 250 mg/kg).

Bronchoalveolar Lavage Fluid (BALF) Collection and Analyses:

Bronchoalveolar lavage fluid (BALF) was collected and quantified as previously described (Hathaway et al. 2021; Majumder et al. 2021a; Majumder et al. 2021b). Briefly, 1 mL of cold sterile PBS was instilled through the trachea and collected. The process was repeated

three times to collect approximately 3 mL of BALF. Total cell number was determined using automated counter Countess II (Invitrogen, Waltham, MA). The cells were centrifuged at 600 rpm at 4 °C for 5 mins and the supernatant was collected and store at −80 °C for further analysis (ELISA, BCA, and LDH Assay). The pelleted cells were resuspended in PBS and processed for Cytospin® (Thermo Fisher Scientific, Waltham, MA) for differential counts and stained with Hema 3 (Fisher Scientific, Pittsburgh, PA). The total protein content in the BALF was quantified using the Pierce BCA Assay kit (Thermo Fisher Scientific, Waltham, MA) as per manufacturer's instructions. The lactate dehydrogenase cytotoxicity assay (LDH) was performed using the LDH Assay Kit (Promega, Madison, WI) as per manufacturer's instructions.

Lung Function Measurement:

The lung function measurements were performed 24 hours post exposure using Scireq Flexivent mechanical ventilator system (SCIREQ, Inc., Montreal, Canada) as described by us previously (Majumder et al. 2021b). The data was recorded using the FlexiWare v8.0 software. Briefly, the mouse was anesthetized with urethane (2 mg/kg), tracheotomized with tracheal cannula (18 gauge, 0.3 cmH2O.s/mL resistance) and mechanically ventilated at 150 breaths/min, tidal volume of 10 ml/kg and a positive end-expiratory pressure (PEEP) of 3 cm H_2O. After two deep inflations (30 cmH_2O pressure), the baseline lung function parameters were measured by applying a broadband forced oscillation waveform (matched to the animal breathing frequency). Data was fitted to a single compartment or constant phase model to obtain the Total Respiratory System Resistance (Rrs) and dynamic compliance (Crs). The Forced Expiratory Volume at 0.1 s (FEV0.1) was measured in triplicates using the NPFEE extension for Flexivent.

Particle Uptake by Macrophages:

Uptake of CB and CB+O_3 particles in the lavage macrophages was assessed to study the extent of interaction between macrophages and particles. This interaction was assessed in terms of 1) % of CB (black aggregates) positive lavage mononuclear cells and, 2) amount of CB uptake (area of the cell occupied by the CB aggregates). At least 500 cells were counted to calculate % CB positive macrophages. Lavage cells (10,000) were spun on slides using Cytospin® (Thermo Fisher Scientific, Waltham, MA) for differential counts and stained with Hema 3 (Fisher Scientific, Pittsburgh, PA). Slides were allowed to dry and coverslips were applied before imaging. A total of 150 cells were imaged for each mouse (approximately ten images per slide) to calculate the area of cell occupied by CB particles (Franca et al. 2011). In total, five mice/slides were analyzed from each treatment group. Each slide was imaged multiple times scanning from bottom to top using Olympus AX70 Microscope (Japan) at 40X magnification. The area of particle uptake in macrophages was analyzed using the ImageJ Fiji software as described previously (Kulkarni et al. 2005). The images were first deconvoluted by using the "Color Deconvolution" function. The images were converted to 8-bit greyscale and then converted to binary images by adjusting the threshold to include the black particles area. The area parameter was analyzed using the "Analyze Particle" function. The total area of the particle positive macrophages was estimated by converting the images to binary images and adjusting the threshold to capture the total cell area in the image. The ROI manager was used to include only the particle positive macrophages for the

analysis. The data was reported and compared as a percentage of area covered by particles in macrophages.

Real-time PCR Gene Expression:

The lung tissues were flash frozen in liquid nitrogen and pulverized over dry ice. The lung tissue powder was further used for RNA extraction and real-time PCR analysis. The RNA extraction was performed using Qiagen Rneasy Mini Kit (Qiagen, Germantown, MD) per manufacturer's recommendations (Qiagen, Germantown, MD). The RNA concentration and purity were measured using Nanodrop. Reverse transcription was performed using the High-Capacity cDNA Reverse Transcription Kit (Thermo Fisher Scientific, Waltham, MA), following manufacturer's recommendation. The Real-Time PCR was performed using AriamaX Real-time PCR System (Agilent, Santa Clara,CA). The relative expression levels were normalized to 18s housekeeping gene using Aria Real-Time PCR Software. Primer sequences are detailed in the Supplemental Table 1.

Enzyme Linked Immunosorbent Assay (ELISA)

ELISA was performed on the bronchoalveolar lavage fluid and lung tissue homogenate to quantify keratinocyte chemoattractant (KC), tumor necrosis factor-α (TNF-α), interleukin-6 (IL-6), interleukin-13 (IL-13), interleukin-1β) (IL-1β) and thymic stromal lymphopoietin (TSLP) using the Duoset sandwich ELISA assay kits (R&D Systems, MN) according to manufacturer's recommendations. The absorbance was read at 450 nm wavelength in Spectramax iD5 plate reader. Lower limit of detection for these assays were IL-1β (15.6 pg/mL), TNF-α (31.3pg/mL), KC (15.6 pg/mL), IL6 (15.6 pg/mL), IL-13 (62.5 pg/mL) and TSLP (15.6 pg/mL).

Lung Burden Quantification:

The lung burden at 24 hours post CB and/or CB+O_3 exposure was quantified 24 hours after a single exposure following a previously published protocol (Elder et al. 2005). Briefly, lungs were kept in a solution of 25% KOH/methanol (w/v) at 60°C heated block overnight, followed by centrifugation. The liquid was carefully decanted and the pellets were resuspended in equal volumes of nitric acid and methanol and kept at 60°C heated block for three hours. This was followed by centrifugation, careful decantation of the supernatants and resuspension of the pellet in 1 mL of 10% NP-40. The standard curve was made using particles and 10% NP-40. The absorbance was measured at 700 nm wavelength.

Hydrogen Peroxide (H_2O_2) Quantification:

The H_2O_2 levels in lung homogenate and serum was quantified using the Amplex™ Red Hydrogen Peroxide/Peroxidase Assay Kit (Thermo Fisher Scientific, Waltham, MA). The lung tissues were flash frozen and pulverized over dry ice followed by lysis using RIPA buffer and 1% protease inhibitor cocktail. The protein extracted from lung tissue and serum samples was reacted with HRP and the Amplex Red dye for 45 minutes at room temperature in dark. The H_2O_2 reacts with the Amplex red dye to form a red fluorescent oxidation product, resorufin. The H_2O_2 levels were quantified by measuring the absorbances at 560 nm wavelength using SpectraMax® iD5 plate reader (Molecular Devices, CA). The obtained

values were normalized to the protein content in the tissue using the Pierce BCA Assay Kit (Thermo Fisher Scientific, Waltham, MA) (Kunovac et al. 2019).

Statistics:

Data are presented as mean ± standard error of mean (SEM) unless mentioned otherwise. Normality of data was determined using either D'Agostino-Person and Shapiro-Wilk test. Statistical differences were calculated using either one-way or two-way Analysis of Variance (ANOVA) followed by Tukey's post-hoc test, or a non-parametric ANOVA followed by Kruskal Wallis post-hoc test using GraphPad® Prism 8.3 (GraphPad Software, San Diego, CA). Differences between groups were considered significant when $P \leq 0.05$. Differences between control and exposed groups are denoted by * while difference between treated groups at the same dose are denoted by #. United States Environmental Protection Agency's Benchmark Dose Software (BMDS) Version 3 (EPA) was used to evaluate the benchmark dose (BMD) response (Filipsson et al. 2003; Haber et al. 2018). The Akaike Information Criterion (AIC) was used for model selection, and the model with the lowest AIC value was used to select the best model between the various models. A change in 1 standard deviation in response rate was used as the benchmark response (BMR Multivariate analysis including pairwise regression analysis, Pearson correlation (r), nonparametric spearman's (ρ), hierarchical clustering analysis (HCA) and principal component analysis (PCA) were performed using JMP version 13 (SAS institute, Cary, NC) (Jolliffe and Cadima 2016; Ringner 2008). Predictive screening was performed using Boot Strap Forest approach (Klimberg 2016). The % contribution from the screening was plotted as a heat map. To avoid the use of laboratory animals for unnecessary duplication of our own recently published information, including published cell count data for only the highest dose group (Table 3) (Hathaway et al. 2021; Majumder et al. 2021a) was used for meta-analysis. Lung tissue gene expression and BALF protein expression assays for the highest dose group were performed again on a pool of banked samples from these studies.

Results:

Aerosol Characteristics:

1. **Realtime monitoring, size distributions and depositions:** Aerosol size distribution were estimated by real time monitoring which confirmed stable aerosol generation at all exposure levels (Figure 1 A). We previously published detailed analyses on aerosol morphology using transmission and scanning electron microscopy (Hathaway et al. 2021; Majumder et al. 2021a; Majumder et al. 2021b). APS-SMPS concurrent measurements (mobility-based quantification) as well as ELPI+ (charge-based measurements) confirmed that CB and CB+O_3 aerosols were not very different and were mainly composed of nano/ultrafine particles. Size distributions are presented in Figure 1B while measured count median diameter and geometric standard deviation are presented in Table 2. Particle number concentrations show a clear dose dependent increase. For low medium and high exposures, Multiple Path Particle Dosimetry (MPPD) model predicted 2.33, 4.87, 9.68 μg deposition for CB and 2.42, 4.87, 9.54 μg total deposited dose for CB+O_3 respectively. Gravimetric estimates (from particles collected onto a filter inside the

inhalation exposure chamber) confirmed aerosol concentrations remained within 5% of the target levels.

2. **Surface characterization and oxidative potentials:** Surface oxygen content measurement by XPS confirmed higher amount of surface oxygen in the case of CB+O_3 (for all the test doses) compared to CB (Figure 2 A). Particles in pristine CB aerosol had 3.5% surface oxygen content while low, medium, and high co-exposure aerosol particles had 8.6%, 5.4% and 5.2% surface oxygen content. Aerosol ability to generate oxidants was evaluated by EPR using spin probe CMH which confirmed highest oxidant generation by the medium and high concentrations while low concentration CB+O_3 and CB produced the lowest oxidant levels (Figure 2 B). Figure 2 C showing the ability of the particles to reduce antioxidant levels in human serum (FRAS assay) further confirmed similar oxidant production potential of the co-exposure particulate. The particulates were more potent at medium and high exposure levels while the low dose and CB ranked the lowest in potency.

Lung Inflammation and Injury.

Lung inflammation was assessed by quantifying cellularity of the BAL fluid and by determining cell differentials. A dose dependence in total cell counts as well as macrophage and neutrophil counts was more evident in the case of co-exposure (Table 3). Co-exposure also demonstrated a greater induction in these indices compared to individual exposures. Both O_3 and CB+O_3 induced increased BAL total protein levels, however, the difference between O_3 and CB+O_3 were only statistically significant at the highest exposure levels (Table 3). Co-exposure significantly induced lung injury (LDH increase in BAL) at medium and high doses while this response was only elicited by O_3 at the highest exposure levels (Table 3). The level of hydrogen peroxide (H_2O_2) in the lung tissue homogenate was significantly elevated by only the co-exposure at the highest tested dose (Table 3).

Lung histopathology was performed to assess the lung injury after exposure to low (2.5 mg/m^3 and 0.5 ppm ozone) and medium (5 mg/m^3 and 1 ppm) doses of CB, O_3 and CB+O_3. Control/air and CB exposed mice had no histopathological alterations though CB-laden macrophages were noted in CB exposed mice at both low and medium exposures (Figure 3 A, B, E). Low dose O_3 alone exposure did not induce any inflammatory cell influx or bronchiolar epithelial necrosis while medium dose O_3 did induce epithelial necrosis without associated cellular inflammation (Figure 3 C, F, inset panel F). Co-exposure at both low and medium dose induced an influx of centriacinar inflammatory cells, mainly neutrophils, and airway epithelial necrosis (Figure 3 D, inset panel D G, inset panel G). Semiquantitative scoring for inflammation and epithelial necrosis is presented in Figure 3 H and I. Macrophage hyperplasia was a feature of only co-exposure and was noted at both low and medium dose exposures (Figure 3 J). Histopathological alterations after the high dose exposures were previously reported (Hathaway et al. 2021; Majumder et al. 2021a).

Benchmark dose (BMD) response modeling was performed on the CB, O_3, and CB+O_3 dose response data using different lung injury and inflammatory responses measured. It is clear from this modeling that inflammation related parameters have lower BMD compared with injury parameters and a clear potentiation is seen with co-exposure (Table 3). We

demonstrate that mixed inhalation exposure to CB and O_3 result in greater biological toxicity as indicated by a significant reduction in BMD. The reduction or increased toxicity observed was true as observed with the BMD calculated for all the pulmonary endpoints evaluated. In case of mixed exposure, CB dose reduces 2.24, 3.25, 21.81 and 12.58 times for BALF LDH, proteins, total cell influx and macrophage influx respectively. Similarly, with O_3 the dose required for a BMD change reduces 2.84, 1.13, 2.30, and 1.36 times for BALF LDH, proteins, total cell influx and macrophage influx respectively for mixed exposures compared to O_3 alone. A lesser decrease in case of O_3 compared to greater magnitude changes in case of CB potentially indicate a greater contribution of O_3 in the observed responses. Principal component analysis (PCA) was performed to interpret the response from each animal from the multidimensional pulmonary injury and inflammation data. PCA of the co-exposure groups clearly indicated a dose dependent response (Figure 4). The response of low and medium concentrations clustered together and was closer to the response of air exposed animals. The high dose exposure, however, had a distinct response from the other two doses. The PCA loading plot further showed BALF LDH and total protein response was akin and the response from BALF PMN influx, BALF AM influx and total cell influx was similar. PCA of all the exposures together presented in Supplemental Figure 1 showed similarity in response with animals exposed to high O_3 and medium dose of co-exposure, similarity in response of air with all doses of CB exposed animals, no change in response between low dose O_3 and low dose co-exposure, and a distinct response with high dose co-exposure.

Co-exposure induced Lung Function Decline

Exposure to both medium (5 mg/m^3 +1 ppm) and high dose (10 mg/m^3 + 2ppm) of CB+O_3 induced a significant increase in respiratory resistance (Rrs), a decrease in dynamic compliance (Crs) and decline in forced expiratory flow at 0.1 s (FEV0.1) in co-exposure animals compared with air (Table 3). However, no change in Rrs and FEV0.1 was observed in lower doses of co-exposure (2.5 mg/m^3 CB + 0.5 ppm O_3) or individual CB and O_3 exposures at any tested dose.

Macrophage Uptake of Particles.

CB uptake was quantified in lavage macrophage by 1) quantifying % of macrophages taking up particles and 2) by quantifying area occupied by CB in each macrophage (Figure 5 A). A dose dependent increase in CB positive BAL macrophages number was observed, while in case CB+O_3 the number of cells was significantly lower than CB at medium and high doses (Figure 5 B). Moreover, no dose dependent increase was observed between medium and high doses. Further, we quantified area per macrophage occupied with CB aggregates and found a dose dependent increase with CB particles that was not observed in the case of CB+O_3 (Figure 5 C).

Lung Carbon Burden after CB and CB+O_3 exposure

Lung burden was quantified 24 hours post exposure and after highest co-exposure (10 mg/m^3 CB + 2 ppm O_3). A significantly greater amount of CB (1.5 ± 0.05 μg/lung) was detected in the lungs of mice after co-exposure compared to the CB alone exposure (0.8 ± 0.08 μg/lung) Figure 5D. At the medium dose co-exposure (5 mg/m^3 CB + 1 ppm O_3), we

detected significant amount of CB in the lungs (1.1± 0.08 μg/lung) of co-exposure mice. However, the CB burden in the CB alone medium exposure was below the detection limit (0.8 μg CB) of our lung burden assay.

Correlation of Aerosol Characteristics with Lung Inflammation/Injury parameters

1. Aerosol Distribution (mobility/charge) and Deposition

Correlations: Different aerosol physicochemical parameters can impact the biological outcome by changing deposition, uptake, and clearance. These relationships have been deciphered in detail for individual toxicants. However, the relative contribution of these parameters in mixed particulate and gas exposures have not been explored. In the current work, using person and spearmen correlation analysis we evaluated the strength of these associations between aerosol physicochemical characteristics and lung inflammation and injury. A comprehensive list of these correlations can be found in the supplemental information (Supplemental Figure 2 and Supplemental File 2). A heatmap based on the correlation coefficient values is presented as Figure 6 A and top significant ($p \leq 0.05$) correlations are highlighted in Figure 6 B. Charge based aerosol size distribution was strongly and positively correlated with total and alveolar lung deposition (r = 0.88, CI (0.756 – 0.945) and BAL total cells (r = 0.71, CI (0.455 – 0.859) and neutrophil counts (r = 0.67, CI (0.403 – 0.842). Another top correlated parameter was total lung deposition that significantly positively correlated with BAL PMN/neutrophils (r = 0.89, CI (0.790 – 0.953), BAL total cells (r = 0.85, CI (0.712 – 0.934), BAL macrophages (r = 0.75, CI (0.530 – 0.883) and BAL LDH (r = 0.59, CI (0.247 – 0.810). Finally, alveolar deposition was significantly positively correlated with BAL PMN/neutrophils (r = 0.89, CI (0.789 – 0.953), BAL total cells (r = 0.85, CI (0.712 – 0.934) and BAL macrophages (r = 0.75, CI (0.530 – 0.883). Similar patterns were obtained by spearman correlation (Supplemental Table 2). All these correlations were statistically significant ($p \leq 0.05$) and absolute significance is presented in Supplemental Table 2.

2. Aerosol Oxidative Potential Correlations:

When particulate have higher oxidation potential, the antioxidants levels in the human serum (used as a test substance) are at a lower level (($p \leq 0.05$) and it correlated with BAL total cells (r = −0.90, CI (0.958 – 0.778), BAL macrophages (r = −0.86, CI (0.943 – 0.712) and BAL PMN/neutrophils (r = 0.86, CI (0.943 – 0.712). Spin probe CMH-based measurements by EPR demonstrated positive and significant ($p \leq 0.05$) correlation with BAL proteins (r = 0.89, CI (0.634 – 0.972), BAL LDH (r = 0.82, CI (0.442 – 0.952) and surface oxygen (r = −0.98, CI (0.998 – 0.938). Particle surface oxygen measurement (XPS) demonstrated negative and significant ($p \leq 0.05$) correlation with BAL total cells (r = − 0.58, CI (0.790 – 0.266), BAL macrophages (r = − 0.57, CI (0.738 – 0.248), and BAL LDH (r = − 0.421, CI (0.710 – 0.011). Similar patterns were obtained by spearman correlation (Supplemental Figure 2, Supplemental Table 2). All these correlations were statistically significant ($p \leq 0.05$) and absolute significance is presented in Supplemental Table 2.

Lung Tissue Gene Expression

Real time PCR based gene expression at the mRNA level was performed on an array of genes. A manual annotation of groups of genes based on known functionality was

performed (Figure 7 A). In line with pulmonary injury and inflammation observed earlier, co-exposure induced gene expression changes were greater in magnitude compared to individual exposures and were more prominent at either lower or higher end of the exposure spectrum. This response was significant ($p \leq 0.05$) except in case of antioxidant genes which show similar induction by both high dose O_3 and CB+O_3. Genes related to alarmin signaling/chronic disease modulation (*Tslp, Il-33, Il-13, Il-13ra1, Il13ra2*), pro-inflammatory response (*Kc, Tnf-α, Il-1β, IL-6*) and mucin (*Muc5ac, Muc5b*) also demonstrated similar pattern. M2 polarization marke rs (*Arg1, Ym1*), usually induced in chronic diseases, were increased at the lowest and highest dose but not at the medium dose while *Tgf-β* was only induced at the lowest dose. Antioxidant response genes (*Nrf2* and *Hmox-1*) were induced maximally at the medium exposure levels for both O_3 and CB+O_3. Interestingly, *IL-13, Tgf-β* and *Tslp* demonstrated more significant mRNA expression induction at the lowest exposure than higher exposures. An HCA approach was also performed for the co-exposure groups to evaluate the grouping of genes based on exposure dose (Figure 7 B). This approach yielded different grouping of genes compared to the literature based functional annotation that is presented in Figure 6A. This approach yielded groups of genes that responded maximally to the lowest dose (*Il-13*, *Tgf-β*, *Tslp* and *Kc*), medium dose (*Muc5b, Il-13ra2, Nrf2,Il-13ra1, Hmox-1*) and the highest dose (*Arg1, Muc5ac,Ym1, Il-33,Il-1β, Muc5b,Il-13ra2,Tnf-α*).

BALF Inflammatory Mediator Secretion and Predictor Screening

An array of mediators was quantified using ELISA assay on BAL fluid. Secretion of all the mediators (IL-13, IL-6, TSLP, KC, IL-1β,TGF-β, TNF-α) was significantly ($p \leq 0.05$) increased by the co-exposure at the highest tested dose (Figure 8 A). Secreted cytokines can be grouped based on distinct patterns of secretion. The first group, which showed enhanced secretion without a clear dose response pattern, consisted of dual function (pro- and anti-inflammatory) cytokines (IL-6, IL-13) and epithelial alarmin TSLP. Interestingly, the greatest increase in IL-13 levels were noted after co-exposure at all the tested co-exposure concentrations. A significant increase (compared to control) in the secretion of IL-6 and IL-13 was also noted by O_3 exposure at the highest exposure level. The second group consisted of typical inflammatory cytokines such as KC, TNF-α, IL-1B and chronic disease modulator TGF-β. These cytokines followed a dose response dependent increase.

Lung tissue homogenate were evaluated for the cytokine/chemokine (IL-13, IL-6, KC and TNF-α) levels (Figure 8 B). A significant increase in all these cytokine/chemokines were seen after highest dose co-exposure (10 mg/m^3 CB + 2 ppm O_3). IL-13 was induced by co-exposure at all the exposure levels, while IL-6 was also induced by O_3 at 2 ppm. This demonstrated a similar trend as lavage ELISA.

A boot strap forest-based machine learning approach was utilized to study the relative contribution of different aerosol characteristics in cytokine production (Figure 8 C). Oxidative status (depletion capacity of the aerosol and lung tissue H_2O_2 levels) was among the significant contributors for IL-1β, KC, and TGF-β secretion while uptake was most significant contributor for the rest of the cytokines.

Discussion:

In this study we aimed at understanding the pulmonary toxicity of ultrafine CB and O_3 inhalation co-exposure at different exposure levels and attempted to determine the correlation/contribution of different physiochemical characteristics in lung injury and inflammation. We demonstrated that co-exposure causes significantly greater pulmonary toxic potential compared to individual exposures as evidenced by sharp decrease in BMD. Quantifying the uptake of the mixtures and evaluating the toxicity showed interesting relationship between uptake and toxicity for mixtures. In addition, using multivariate analysis we elaborate the correlation of physicochemical and oxidative characteristics of the mixtures to pulmonary injury and inflammation. A boot strap forest approach predicted relative contribution of different physiochemical characteristics on the response of individual cytokines measured.

We previously described mechanisms of lung inflammation and lung function decline after inhalation co-exposure to CB and O_3 (Majumder et al. 2021a). The particle dose in that study was equivalent to an alveolar deposited dose of a worker after 8 hours exposure at the current United States Occupational Safety and Health Administration (OSHA) permissible exposure limit (3.5 mg/m^3) (Majumder et al. 2021a). This dose translated to 35 days of PM 2.5 exposures at current national ambient air quality standard (35 μg/m^3). In addition, a 2-ppm dose was selected for exposure to O_3 alone that is 4 times the dose capable of inducing neutrophilia in humans. This selection was made keeping in consideration differences in deposition due to differences in human and murine anatomy (Hatch et al. 2013; Hatch et al. 1994). However, here we report additional findings to considerably lower concentrations of both CB (equivalent exposure of 17.5 and 8.75 days of PM 2.5 exposure at current permissible concentrations) and O_3 exposures at 2 times and same dose that induces neutrophilia). Thus, utilizing more relevant exposure concentrations, we are providing a detailed evaluation of co-exposure responsive lung inflammatory and injury markers as well as describe the correlations of different aerosol characteristics with lung toxicity.

Our findings of increased CB retention in the lung in case of CB and O_3 co-exposure indicate the possibility of persistent adverse outcomes as retention of particulates in the lungs has been linked to chronic pulmonary phenotypes in case of a variety of environmental exposures and engineered nanoparticle exposures (Fraser et al. 2021; Oberdorster et al. 2015; Oberdorster et al. 1994; Riediker et al. 2019). Furthermore, as this co-exposure particles can produce more reactive oxygen species (detected in the lungs and systemic circulation) this increase the possibility of aggravating systemic diseases and for an extended period. Lung function data confirms the changes in functional respiratory parameters (Rrs, Crs and FEV0.1) after exposure to medium and high co-exposure concentrations while individual exposures and low dose co-exposure did not induce any functional change. These observations at the highest dose exposures are in line with our recently published study using a similar dose (Majumder et al. 2021a). This data clearly points towards a greater functional impact of co-exposure compared to individual exposures at medium and high doses.

The dose response data was used to determine relative potency of the test aerosols using BMD modeling. The BMD approach is statistically more robust and resulting values are inherently less uncertain than other dose response metrics. This approach has been used to understand responses of other inhaled particulate pollutants (engineered nanomaterials and fibers) (Kuempel et al. 2006; O'Brien and Cummins 2010; Pink et al. 2020; Weldon et al. 2018). Here, we describe a significant reduction in both CB and O_3 dose in the case of mixed exposures which confirms our previous findings of increased biological activity of mixed CB and O_3 exposure compared to single toxicant exposures (Hathaway et al. 2021; Majumder et al. 2021a).

Uptake of particulate materials (particulate matter, engineered nanoparticles) in most of the cases is considered essential for biological activity (Hussain et al. 2009; Maynard et al. 2006; Patel et al. 2015; Zheng et al. 2018). We previously demonstrated that after O_3-reacted CB particle exposure, macrophages released CXCR3 receptor ligands that play an important role in the endothelial cell responses (impaired scratch healing and monolayer permeability) (Majumder et al. 2021b). Here, in case of CB exposure alone, we observed a linear increase in % macrophages in lavage that take up the particulate. However, in the case of co-exposure this response plateaued with medium and high dose. At these two doses there was not a significant increase in % macrophages that take up the particulate. When compared with CB, in the CB+O_3 group, a significantly smaller number of macrophages were detected to contain CB aggregates at medium and high exposure levels. The increase in toxicity and plateau of uptake suggests increase biological potency and a differential surface reactivity of the co-exposure aerosols. While we observe that similar characteristics are involved in single and co-exposure outcomes, it important to note that the potency is significantly enhanced. Surface reactivity can be deduced from the acellular assays such as oxidant generation capacity (EPR study using spin probe CMH) and reduction of antioxidants in human serum (FRAS assay). These findings further corroborate the conclusion that interaction with O_3 increased surface reactivity of CB particles. However, it is important to note that while both medium and high exposures produced similar oxidant levels by EPR analysis, FRAS assay indicated a dose dependent antioxidant depletion. Multiple published reports confirm the utility of FRAS assay in detecting the oxidative potential of the particulate materials (Fraser et al. 2020; Rogers et al. 2008). Moreover, it is important to note that we recently demonstrated that reactive oxygen species generation is a critical factor behind enhanced biological activity of the co-exposure (Hathaway et al. 2021; Majumder et al. 2021a; Majumder et al. 2021b). Thus, in case of mixed exposures, while we are seeing similar physicochemical characteristics involved in toxic response, oxidant dependence is significantly greater.

Increasing concentration of mixed exposures leads to a decrease in the CB aggregate area in macrophages, while a dose dependent increase was observed in the case of CB alone. A potential explanation of this change is increased toxicity leading to macrophage cell death. Indeed, we observed increased LDH release with increasing co-exposure doses. Previous literature confirms increased toxicity of macrophages after exposure to varied air pollutants including PM, O_3 and ultrafine/nanoparticles (Devlin et al. 1994; Gowdy et al. 2021; Patial and Saini 2020; Sunil et al. 2012; Wei et al. 2021; Wottrich et al. 2004). However, the increase in LDH could be due to toxicity of several cell types including epithelial cells

and non-mono-nuclear cells (neutrophils *etc.,*). A potential reduction in phagocytic ability due to the co-exposure can also result in similar result. Particulate exposures are known to impact the uptake mechanisms which can result in altered bacteria/virus uptake (Hussain et al. 2009; Pacheco et al. 2013; Vranic et al. 2013). This can have serious consequences in terms of clearance of a later infection and mounting an effective immune response. Work is currently being performed to further elaborate on these mechanisms. However, as demonstrated by us previously and in this manuscript, there is an increased ROS production in the lungs. Oxidant generation can lead to reduced phagocytic ability (Anderson et al. 2002) and cell death (Hussain et al. 2010). We previously demonstrated that uptake of CB particles in the epithelial cells occur by both energy dependent and independent processes and recently reported a decrease in ATP production after CB and O_3 co-exposure (Hathaway et al. 2021). A consequence of these processes is an increased lung burden of CB in case of O_3 (co-exposure scenario) clearly indicating greater retention of CB in the lungs. Alternatively, the reduction in uptake at higher doses can potentially be a homeostatic/protective mechanism induced due to alterations in the cellular metabolic state (Caceres et al. 2020). The Ym1 and Arg1 are M2 phenotype markers and M2 macrophages have been shown to express higher phagocytosis abilities (Schulz et al. 2019). This potentially indicates a homeostatic response to clear the particles. The impacts on macrophage death/survival and endocytosis abilities can happen together or independent of each other. Further studies are ongoing to elaborate the mechanisms involved in these processes.

Apart from pulmonary injury and inflammation, we showed significant alteration in mRNA and protein secretions with co-exposures compared to single exposures. An enhanced biological activity of co-exposure compared to individual exposures was evident even at the lowest dose for *Tslp*, *Il-13*, *Tgf-β* and *Il-1β*. These genes are known to play an important role in chronic pulmonary disorders such as asthma, chronic obstructive pulmonary disease (COPD), and fibrosis (Kabesch et al. 2006; Verma et al. 2018; Wang et al. 2018). In general, co-exposure induced gene expression changes were more prominent at either the lower or higher end of the exposure spectrum. Antioxidant response genes (*Hmox-1* and *Nrf-2*) did not follow the pattern of the earlier genes. *Nrf-2* is a master regulator of cellular antioxidant defenses and is known to play an important role in O_3 induced pulmonary damage (Cervellati et al. 2020; Cho et al. 2013; Henriquez et al. 2017). *Hmox-1* is an antioxidant enzyme induced by a multitude of oxidative stimuli and is also implicated in O_3 induced (Li et al. 2000; Takahashi et al. 1997). The antioxidant response genes did not induce greater gene expression compared to individual exposures. This could be due to an impaired capacity of the lungs to mount an antioxidant response after co-exposures. Taken together, we saw an increased antioxidant depletion capacity and greater H_2O_2 production with co-exposures, translating into a more serious oxidative imbalance. Oxidative imbalances play a significant role in air pollution induced toxicity as well as in the pathogenesis of multiple chronic disorders that are exacerbated by air pollution (Ambroz et al. 2016; Domej et al. 2014; Kelly and Fussell 2017). Lung has a complex architecture including multiple cell types and a myriad of other components that can influence redox balance including glutathione, lipids, and surfactants. In the current work we have evaluated the pulmonary damage, inflammation and uptake using recovered bronchoalveolar lavage fluid and a broader pathological understanding is needed to fully understand the alterations

occurring at the organ level. Although macrophages are the primary responders involved in particle clearance and as such the uptake was evaluated in recovered alveolar macrophages from bronchoalveolar lavage fluid, more work is warranted to understand the uptake by other cell types and evaluate spatial interactions with various redox elements present in the lung.

Our results collectively point towards a chronic disease conducive phenotype i.e., over expression of M2 macrophage markers (Arg1 and Ym1), Mucin genes (Muc5b and Muc5c) and IL-13 secretion. These findings corroborate the findings of increased IL-13 levels after air pollution exposure and their potential role in chronic disease susceptibility (Nadeau et al. 2010; Pourazar et al. 2004; Williams et al. 2008). In addition, these results have a mechanistic aspect as IL-13 is known inducer of mucin genes, M2 macrophage phenotype and Th2 dominated immune response in chronic respiratory diseases such as asthma and COPD (de Vries 1998; Duffield 2003; McKenzie et al. 1993).

Our study has multiple strengths including a realistic co-exposure system and model, use of multiple doses of O_3 and CB ranging from occupational to environmental exposure scenarios providing relevant deposition levels, use of statistical approaches to identify the correlation of biological outcomes with aerosol physicochemical characteristics, use of a BMD approach for ranking of exposures, and evaluation of multiple readouts for inflammation and injury. However, our study does have some limitations that include use of male mice only, use of fixed ratio for CB and O_3, and use of single exposure at relatively higher exposure concentration rather than a chronic exposure scenario. We observed a discordance between the mRNA expression and protein expression levels. Genome wide research conducted over the last two decades showed although correlation exists between mRNA and protein expression levels, and such patterns are far from perfect. This could be due to various factors including transcription to translational defects, post translational modifications, cyclic expression with check points and due to timing lag between mRNA and protein expression. Further expansive temporal studies are required to decipher these interesting trends and such studies will hopefully elaborate the differentially observed effects.

In conclusion, the BMD of the pulmonary injury and inflammation response demonstrates that inhalation co-exposure to CB and O_3 result in greater pulmonary toxicity compared to individual CB or O_3 exposures. Interestingly, the uptake of the particulate was suppressed with an increasing dose of the CB + O_3 mixture, but the toxicity escalated with increasing dose of the mixture, suggesting that the particles from CB + O_3 mixtures at higher dose were more potent in inducing toxicity. We also identified aerosol physicochemical characteristics of the mixtures that correlated with biological outcomes and predict the relative contribution of these parameters on individual inflammatory cytokine secretions. Our results indicate a greater modulation of chronic disease mediators by the co-exposure at the lowest tested levels that indicate a greater potential to exacerbate chronic pulmonary disease. Further research is underway with even more reduced levels of both CB and O_3 as well as using animal models of respiratory disorders to further investigate the pathophysiological impacts of co-exposure. With this study and our recent work, we have detailed the interactive outcomes after ultrafine CB and O_3 inhalation exposure. Future studies should investigate

the impact of different mixing ratio of O_3 and CB and chronic exposure at ambient levels to further elucidate the interactive outcomes in this exposure model.

Supplementary Material

Refer to Web version on PubMed Central for supplementary material.

Acknowledgements

Authors are grateful for excellent help by Dr. James Wagner (MSU) for histopathology and for technical assistance by Kevin Engels, Zirong (Sherry) Xie, Tom Batchelor and Qiang Wang.

Funding Statement

This study was supported by National Institute of Health funding R01 ES031253 (SH), NIGMS U54GM104942 (SH), R01 ES015022 (TRN), R01 DK124510 (EEK), P20 GM109098 (EEK), NIA R56 NS117754 (EEK), and NIOSH NTRC # 9390BN6 (VK).

Abbreviations:

PS	Aerosol particle sizer
Arg1	Arginase 1
BALF	Bronchoalveolar lavage fluid
BMD	Benchmark Dose
CB	Carbon Black
CMH	1-hydroxy-3-carboxymethyl-2,2,5,5-tetramethyl-pyrrolidine
ELPI	Electrical low-pressure impactor
EPR	Electron Paramagnetic Resonance
FRAS	Ferric Reducing Ability of Serum
Hmox1	Heme Oxygenase 1
IL-13	Iterleukin-13
Il-13ra1	Interleukin-13 receptor subunit alpha 1
Il-13ra2	Interle2kin-13 receptor subunit alpha 1
IL-1β	Interleukin-1β
IL-6	Interleukin-6
KC	Keratinocyte chemoattractant
MPPD	Multiple Path Particle Dosimetry
Muc5ac	Mucin 5a

Muc5b	Mucin 5b
Nrf2	Nuclear factor-erythroid factor 2-related factor 2
O_3	Ozone
PCA	Principal component analyses
PM 2.5	Particulate matter 2.5
SMPS	Scanning mobility particle sizer
TGF-β	Transforming growth factor beta
TNF- α	Tumor necrosis factor-α
TSLP	Thymic stromal lymphopoietin
XPS	X-Ray Photo Electron Spectroscopy

References

Ambroz A, Vlkova V, Rossner P Jr., Rossnerova A, Svecova V, Milcova A, Pulkrabova J, Hajslova J, Veleminsky M Jr., Solansky I et al. 2016. Impact of air pollution on oxidative DNA damage and lipid peroxidation in mothers and their newborns. Int J Hyg Environ Health. 219(6):545–556. [PubMed: 27321041]

Anderson HA, Englert R, Gursel I, Shacter E. 2002. Oxidative stress inhibits the phagocytosis of apoptotic cells that have externalized phosphatidylserine. Cell Death Differ. 9(6):616–625. [PubMed: 12032670]

Anenberg SC, West JJ, Yu HB, Chin M, Schulz M, Bergmann D, Bey I, Bian HS, Diehl T, Fiore A et al. 2014. Impacts of intercontinental transport of anthropogenic fine particulate matter on human mortality. Air Qual Atmos Hlth. 7(3):369–379.

Apte JS, Marshall JD, Cohen AJ, Brauer M. 2015. Addressing global mortality from ambient pm2.5. Environmental Science & Technology. 49(13):8057–8066. [PubMed: 26077815]

Birnbaum HG, Carley CD, Desai U, Ou S, Zuckerman PR. 2020. Measuring the impact of air pollution on health care costs. Health Aff (Millwood). 39(12):2113–2119. [PubMed: 33284710]

Braakhuis HM, Park MV, Gosens I, De Jong WH, Cassee FR. 2014. Physicochemical characteristics of nanomaterials that affect pulmonary inflammation. Part Fibre Toxicol. 11:18. [PubMed: 24725891]

Caceres L, Paz ML, Garces M, Calabro V, Magnani ND, Martinefski M, Adami PVM, Caltana L, Tasat D, Morelli L et al. 2020. Nadph oxidase and mitochondria are relevant sources of superoxide anion in the oxinflammatory response of macrophages exposed to airborne particulate matter. Ecotox Environ Safe 205.

Campen MJ, Buntz J, Lund A, Seagrave J, Vedal S, Mauderly J, McDonald J. 2009. Vascular effects of vapor and particulate phases of traffic-related air pollution: Initial results from the npact initiative. Am J Resp Crit Care. 179.

Cervellati F, Woodby B, Benedusi M, Ferrara F, Guiotto A, Valacchi G. 2020. Evaluation of oxidative damage and nrf2 activation by combined pollution exposure in lung epithelial cells. Environ Sci Pollut Res Int. 27(25):31841–31853. [PubMed: 32504424]

Cho HY, Gladwell W, Yamamoto M, Kleeberger SR. 2013. Exacerbated airway toxicity of environmental oxidant ozone in mice deficient in nrf2. Oxid Med Cell Longev. 2013:254069. [PubMed: 23766849]

Cleary EG, Cifuentes M, Grinstein G, Brugge D, Shea TB. 2018. Association of low-level ozone with cognitive decline in older adults. J Alzheimers Dis. 61(1):67–78. [PubMed: 29103040]

de Vries JE. 1998. The role of il-13 and its receptor in allergy and inflammatory responses. J Allergy Clin Immunol. 102(2):165–169. [PubMed: 9723655]

Devlin RB, McKinnon KP, Noah T, Becker S, Koren HS. 1994. Ozone-induced release of cytokines and fibronectin by alveolar macrophages and airway epithelial cells. Am J Physiol. 266(6 Pt 1):L612–619. [PubMed: 8023949]

Domej W, Oettl K, Renner W. 2014. Oxidative stress and free radicals in copd--implications and relevance for treatment. Int J Chron Obstruct Pulmon Dis. 9:1207–1224. [PubMed: 25378921]

Duffield JS. 2003. The inflammatory macrophage: A story of jekyll and hyde. Clin Sci (Lond). 104(1):27–38. [PubMed: 12519085]

Elder A, Gelein R, Finkelstein JN, Driscoll KE, Harkema J, Oberdorster G. 2005. Effects of subchronically inhaled carbon black in three species. I. Retention kinetics, lung inflammation, and histopathology. Toxicol Sci. 88(2):614–629. [PubMed: 16177241]

EPA. Benchmark dose software (bmds). United states environmental protection agency.

Farhat SCL, Almeida MB, Silva-Filho L, Farhat J, Rodrigues JC, Braga ALF. 2013. Ozone is associated with an increased risk of respiratory exacerbations in patients with cystic fibrosis. Chest. 144(4):1186–1192. [PubMed: 23493973]

Fauroux B, Sampil M, Quenel P, Lemoullec Y. 2000. Ozone: A trigger for hospital pediatric asthma emergency room visits. Pediatr Pulmonol. 30(1):41–46. [PubMed: 10862161]

Filipsson AF, Sand S, Nilsson J, Victorin K. 2003. The benchmark dose method--review of available models, and recommendations for application in health risk assessment. Crit Rev Toxicol. 33(5):505–542. [PubMed: 14594105]

Franca A, Aggarwal P, Barsov EV, Kozlov SV, Dobrovolskaia MA, Gonzalez-Fernandez A. 2011. Macrophage scavenger receptor a mediates the uptake of gold colloids by macrophages in vitro. Nanomedicine (Lond). 6(7):1175–1188. [PubMed: 21675859]

Fraser K, Hubbs A, Yanamala N, Mercer RR, Stueckle TA, Jensen J, Eye T, Battelli L, Clingerman S, Fluharty K et al. 2021. Histopathology of the broad class of carbon nanotubes and nanofibers used or produced in u.S. Facilities in a murine model. Part Fibre Toxicol. 18(1):47. [PubMed: 34923995]

Fraser K, Kodali V, Yanamala N, Birch ME, Cena L, Casuccio G, Bunker K, Lersch TL, Evans DE, Stefaniak A et al. 2020. Physicochemical characterization and genotoxicity of the broad class of carbon nanotubes and nanofibers used or produced in u.S. Facilities. Part Fibre Toxicol. 17(1):62. [PubMed: 33287860]

GBDCRD C. 2017. Global, regional, and national deaths, prevalence, disability-adjusted life years, and years lived with disability for chronic obstructive pulmonary disease and asthma, 1990–2015: A systematic analysis for the global burden of disease study 2015. Lancet Respir Med. 5(9):691–706. [PubMed: 28822787]

GBDRFC C. 2016. Global, regional, and national comparative risk assessment of 79 behavioural, environmental and occupational, and metabolic risks or clusters of risks, 1990–2015: A systematic analysis for the global burden of disease study 2015. Lancet. 388(10053):1659–1724. [PubMed: 27733284]

Ghosh R, Causey K, Burkart K, Wozniak S, Cohen A, Brauer M. 2021. Ambient and household pm2.5 pollution and adverse perinatal outcomes: A meta-regression and analysis of attributable global burden for 204 countries and territories. PLoS Med. 18(9):e1003718. [PubMed: 34582444]

Gowdy KM, Kilburg-Basnyat B, Hodge MX, Reece SW, Yermalitsk V, Davies SS, Manke J, Armstrong ML, Reisdorph N, Tighe RM et al. 2021. Novel mechanisms of ozone-induced pulmonary inflammation and resolution, and the potential protective role of scavenger receptor bi. Res Rep Health Eff Inst. (204):1–49.

Haber LT, Dourson ML, Allen BC, Hertzberg RC, Parker A, Vincent MJ, Maier A, Boobis AR. 2018. Benchmark dose (bmd) modeling: Current practice, issues, and challenges. Crit Rev Toxicol. 48(5):387–415. [PubMed: 29516780]

Hamade AK, Misra V, Rabold R, Tankersley CG. 2010. Age-related changes in cardiac and respiratory adaptation to acute ozone and carbon black exposures: Interstrain variation in mice. Inhal Toxicol 22 Suppl 2:84–94.

Hamade AK, Rabold R, Tankersley CG. 2008. Adverse cardiovascular effects with acute particulate matter and ozone exposures: Interstrain variation in mice. Environ Health Perspect. 116(8):1033–1039. [PubMed: 18709144]

Harber P, Muranko H, Solis S, Torossian A, Merz B. 2003. Effect of carbon black exposure on respiratory function and symptoms. J Occup Environ Med. 45(2):144–155. [PubMed: 12625230]

Hatch GE, McKee J, Brown J, McDonnell W, Seal E, Soukup J, Slade R, Crissman K, Devlin R. 2013. Biomarkers of dose and effect of inhaled ozone in resting versus exercising human subjects: Comparison with resting rats. Biomark Insights. 8:53–67. [PubMed: 23761957]

Hatch GE, Slade R, Harris LP, McDonnell WF, Devlin RB, Koren HS, Costa DL, McKee J. 1994. Ozone dose and effect in humans and rats. A comparison using oxygen-18 labeling and bronchoalveolar lavage. Am J Respir Crit Care Med. 150(3):676–683. [PubMed: 8087337]

Hathaway QA, Majumder N, Goldsmith WT, Kunovac A, Pinti MV, Harkema JR, Castranova V, Hollander JM, Hussain S. 2021. Transcriptomics of single dose and repeated carbon black and ozone inhalation co-exposure highlight progressive pulmonary mitochondrial dysfunction. Part Fibre Toxicol. 18(1):44. [PubMed: 34911549]

Henriquez A, House J, Miller DB, Snow SJ, Fisher A, Ren H, Schladweiler MC, Ledbetter AD, Wright F, Kodavanti UP. 2017. Adrenal-derived stress hormones modulate ozone-induced lung injury and inflammation. Toxicol Appl Pharmacol. 329:249–258. [PubMed: 28623178]

Holz O, Heusser K, Muller M, Windt H, Schwarz K, Schindler C, Tank J, Hohlfeld JM, Jordan J. 2018. Airway and systemic inflammatory responses to ultrafine carbon black particles and ozone in older healthy subjects. J Toxicol Environ Health A. 81(13):576–588. [PubMed: 29693510]

Hussain S, Boland S, Baeza-Squiban A, Hamel R, Thomassen LC, Martens JA, Billon-Galland MA, Fleury-Feith J, Moisan F, Pairon JC et al. 2009. Oxidative stress and proinflammatory effects of carbon black and titanium dioxide nanoparticles: Role of particle surface area and internalized amount. Toxicology. 260(1–3):142–149. [PubMed: 19464580]

Hussain S, Thomassen LC, Ferecatu I, Borot MC, Andreau K, Martens JA, Fleury J, Baeza-Squiban A, Marano F, Boland S. 2010. Carbon black and titanium dioxide nanoparticles elicit distinct apoptotic pathways in bronchial epithelial cells. Part Fibre Toxicol. 7:10. [PubMed: 20398356]

Jolliffe IT, Cadima J. 2016. Principal component analysis: A review and recent developments. Philos Trans A Math Phys Eng Sci. 374(2065):20150202. [PubMed: 26953178]

Kabesch M, Schedel M, Carr D, Woitsch B, Fritzsch C, Weiland SK, von Mutius E. 2006. Il-4/il-13 pathway genetics strongly influence serum ige levels and childhood asthma. J Allergy Clin Immunol. 117(2):269–274. [PubMed: 16461126]

Kelly FJ, Fussell JC. 2017. Role of oxidative stress in cardiovascular disease outcomes following exposure to ambient air pollution. Free Radic Biol Med. 110:345–367. [PubMed: 28669628]

Klimberg RaM BD,. 2016. Fundamentals of predictive analytics with jmp. Sas institute.

Kuempel ED, Tran CL, Castranova V, Bailer AJ. 2006. Lung dosimetry and risk assessment of nanoparticles: Evaluating and extending current models in rats and humans. Inhal Toxicol. 18(10):717–724. [PubMed: 16774860]

Kulkarni NS, Prudon B, Panditi SL, Abebe Y, Grigg J. 2005. Carbon loading of alveolar macrophages in adults and children exposed to biomass smoke particles. Sci Total Environ. 345(1–3):23–30. [PubMed: 15919524]

Kunovac A, Hathaway QA, Pinti MV, Goldsmith WT, Durr AJ, Fink GK, Nurkiewicz TR, Hollander JM. 2019. Ros promote epigenetic remodeling and cardiac dysfunction in offspring following maternal engineered nanomaterial (enm) exposure. Part Fibre Toxicol. 16(1):24. [PubMed: 31215478]

Li L, Hamilton RF, Holian A 2000. Protection against ozone-induced pulmonary inflammation and cell death by endotoxin pretreatment in mice: Role of ho-1. Inhal Toxicol. 12(12):1225–1238. [PubMed: 11203434]

Majumder N, Goldsmith WT, Kodali VK, Velayutham M, Friend SA, Khramtsov VV, Nurkiewicz TR, Erdely A, Zeidler-Erdely PC, Castranova V et al. 2021a. Oxidant-induced epithelial alarmin pathway mediates lung inflammation and functional decline following ultrafine carbon and ozone inhalation co-exposure. Redox Biol. 46:102092. [PubMed: 34418598]

Majumder N, Velayutham M, Bitounis D, Kodali VK, Hasan Mazumder MH, Amedro J, Khramtsov VV, Erdely A, Nurkiewicz T, Demokritou P et al. 2021b. Oxidized carbon black nanoparticles induce endothelial damage through c-x-c chemokine receptor 3-mediated pathway. Redox Biol. 47:102161. [PubMed: 34624601]

Mauderly JL, Samet JM. 2009. Is there evidence for synergy among air pollutants in causing health effects? Environ Health Persp. 117(1):1–6.

Maynard AD, Aitken RJ, Butz T, Colvin V, Donaldson K, Oberdorster G, Philbert MA, Ryan J, Seaton A, Stone V et al. 2006. Safe handling of nanotechnology. Nature. 444(7117):267–269. [PubMed: 17108940]

McKenzie AN, Culpepper JA, de Waal Malefyt R, Briere F, Punnonen J, Aversa G, Sato A, Dang W, Cocks BG, Menon S et al. 1993. Interleukin 13, a t-cell-derived cytokine that regulates human monocyte and b-cell function. Proc Natl Acad Sci U S A. 90(8):3735–3739. [PubMed: 8097324]

Nadeau K, McDonald-Hyman C, Noth EM, Pratt B, Hammond SK, Balmes J, Tager I. 2010. Ambient air pollution impairs regulatory t-cell function in asthma. J Allergy Clin Immunol. 126(4):845–852 e810. [PubMed: 20920773]

Nurkiewicz TR, Porter DW, Hubbs AF, Cumpston JL, Chen BT, Frazer DG, Castranova V. 2008. Nanoparticle inhalation augments particle-dependent systemic microvascular dysfunction. Part Fibre Toxicol. 5:1. [PubMed: 18269765]

O'Brien N, Cummins E. 2010. Ranking initial environmental and human health risk resulting from environmentally relevant nanomaterials. J Environ Sci Health A Tox Hazard Subst Environ Eng. 45(8):992–1007. [PubMed: 20486008]

Oberdorster G, Castranova V, Asgharian B, Sayre P. 2015. Inhalation exposure to carbon nanotubes (cnt) and carbon nanofibers (cnf): Methodology and dosimetry. J Toxicol Environ Health B Crit Rev. 18(3–4):121–212. [PubMed: 26361791]

Oberdorster G, Ferin J, Lehnert BE. 1994. Correlation between particle size, in vivo particle persistence, and lung injury. Environ Health Perspect. 102 Suppl 5:173–179.

Organization WH. 2016. World health statistics 2016: Monitoring health for the sdgs https://www.Who.Int/gho/publications/world_health_statistics/2016/annex_b/en/ accessed 14 january, 2019.

Pacheco P, White D, Sulchek T. 2013. Effects of microparticle size and fc density on macrophage phagocytosis. PLoS One. 8(4):e60989. [PubMed: 23630577]

Patel B, Gupta N, Ahsan F. 2015. Particle engineering to enhance or lessen particle uptake by alveolar macrophages and to influence the therapeutic outcome. Eur J Pharm Biopharm. 89:163–174. [PubMed: 25497488]

Patial S, Saini Y. 2020. Lung macrophages: Current understanding of their roles in ozone-induced lung diseases. Crit Rev Toxicol. 50(4):310–323. [PubMed: 32458707]

Pink M, Verma N, Schmitz-Spanke S. 2020. Benchmark dose analyses of toxic endpoints in lung cells provide sensitivity and toxicity ranking across metal oxide nanoparticles and give insights into the mode of action. Toxicol Lett. 331:218–226. [PubMed: 32562635]

Pirela SV, Martin J, Bello D, Demokritou P. 2017. Nanoparticle exposures from nano-enabled toner-based printing equipment and human health: State of science and future research needs. Crit Rev Toxicol. 47(8):678–704. [PubMed: 28524743]

Pourazar J, Frew AJ, Blomberg A, Helleday R, Kelly FJ, Wilson S, Sandstrom T. 2004. Diesel exhaust exposure enhances the expression of il-13 in the bronchial epithelium of healthy subjects. Respir Med. 98(9):821–825. [PubMed: 15338792]

Rattanasom N, Saowapark Ta, Deeprasertkul C. 2007. Reinforcement of natural rubber with silica/carbon black hybrid filler. Polymer Testing. 26(3):369–377.

Rhee J, Dominici F, Zanobetti A Schwartz J Wang J, Di Q, Christiani DC,. 2018. The imapct of long-term exposure to pm2.5 and ozone on the risk of acute respiratory distress syndrome (ards) for elderly. Am J Respir Crit Care Med. 197:A6192.

Riediker M, Zink D, Kreyling W, Oberdorster G, Elder A, Graham U, Lynch I, Duschl A, Ichihara G, Ichihara S et al. 2019. Particle toxicology and health - where are we? Part Fibre Toxicol. 16(1):19. [PubMed: 31014371]

Ringner M 2008. What is principal component analysis? Nat Biotechnol. 26(3):303–304. [PubMed: 18327243]

Rogers EJ, Hsieh SF, Organti N, Schmidt D, Bello D. 2008. A high throughput in vitro analytical approach to screen for oxidative stress potential exerted by nanomaterials using a biologically relevant matrix: Human blood serum. Toxicol In Vitro. 22(6):1639–1647. [PubMed: 18593597]

Schulz D, Severin Y, Zanotelli VRT, Bodenmiller B. 2019. In-depth characterization of monocyte-derived macrophages using a mass cytometry-based phagocytosis assay. Sci Rep. 9(1):1925. [PubMed: 30760760]

Shehab MA, Pope FD. 2019. Effects of short-term exposure to particulate matter air pollution on cognitive performance. Sci Rep. 9(1):8237. [PubMed: 31160655]

Shin SW, Song IH, Um SH. 2015. Role of physicochemical properties in nanoparticle toxicity. Nanomaterials (Basel). 5(3):1351–1365. [PubMed: 28347068]

Singh D, Marrocco A, Wohlleben W, Park HR, Diwadkar AR, Himes BE, Lu Q, Christiani DC, Demokritou P. 2022. Release of particulate matter from nano-enabled building materials (nebms) across their lifecycle: Potential occupational health and safety implications. J Hazard Mater. 422:126771. [PubMed: 34391975]

Sunil VR, Patel-Vayas K, Shen J, Laskin JD, Laskin DL. 2012. Classical and alternative macrophage activation in the lung following ozone-induced oxidative stress. Toxicol Appl Pharmacol. 263(2):195–202. [PubMed: 22727909]

Takahashi Y, Takahashi S, Yoshimi T, Miura T, Mochitate K, Kobayashi T. 1997. Increases in the mrna levels of gamma-glutamyltransferase and heme oxygenase-1 in the rat lung after ozone exposure. Biochem Pharmacol. 53(7):1061–1064. [PubMed: 9174121]

Verma M, Liu S, Michalec L, Sripada A, Gorska MM, Alam R. 2018. Experimental asthma persists in il-33 receptor knockout mice because of the emergence of thymic stromal lymphopoietin-driven il-9(+) and il-13(+) type 2 innate lymphoid cell subpopulations. J Allergy Clin Immunol. 142(3):793–803 e798. [PubMed: 29132961]

Vranic S, Boggetto N, Contremoulins V, Mornet S, Reinhardt N, Marano F, Baeza-Squiban A, Boland S. 2013. Deciphering the mechanisms of cellular uptake of engineered nanoparticles by accurate evaluation of internalization using imaging flow cytometry. Part Fibre Toxicol. 10:2. [PubMed: 23388071]

Wagner JG, Allen K, Yang HY, Nan B, Morishita M, Mukherjee B, Dvonch JT, Spino C, Fink GD, Rajagopalan S et al. 2014. Cardiovascular depression in rats exposed to inhaled particulate matter and ozone: Effects of diet-induced metabolic syndrome. Environ Health Perspect. 122(1):27–33. [PubMed: 24169565]

Wang W, Li Y, Lv Z, Chen Y, Li Y, Huang K, Corrigan CJ, Ying S. 2018. Bronchial allergen challenge of patients with atopic asthma triggers an alarmin (il-33, tslp, and il-25) response in the airways epithelium and submucosa. J Immunol. 201(8):2221–2231. [PubMed: 30185520]

Wei H, Yuan W, Yu H, Geng H. 2021. Cytotoxicity induced by fine particulate matter (pm2.5) via mitochondria-mediated apoptosis pathway in rat alveolar macrophages. Environ Sci Pollut Res Int. 28(20):25819–25829. [PubMed: 33474668]

Weldon BA, Griffith WC, Workman T, Scoville DK, Kavanagh TJ, Faustman EM. 2018. In vitro to in vivo benchmark dose comparisons to inform risk assessment of quantum dot nanomaterials. Wiley Interdiscip Rev Nanomed Nanobiotechnol. 10(4):e1507. [PubMed: 29350469]

Williams AS, Nath P, Leung SY, Khorasani N, McKenzie AN, Adcock IM, Chung KF. 2008. Modulation of ozone-induced airway hyperresponsiveness and inflammation by interleukin-13. Eur Respir J. 32(3):571–578. [PubMed: 18417511]

Wilson A, Reich BJ, Nolte CG, Spero TL, Hubbell B, Rappold AG. 2017. Climate change impacts on projections of excess mortality at 2030 using spatially varying ozone-temperature risk surfaces. J Expo Sci Environ Epidemiol. 27(1):118–124. [PubMed: 27005744]

Wong EM, Walby WF, Wilson DW, Tablin F, Schelegle ES. 2018. Ultrafine particulate matter combined with ozone exacerbates lung injury in mature adult rats with cardiovascular disease. Toxicol Sci. 163(1):140–151. [PubMed: 29394414]

Wottrich R, Diabate S, Krug HF. 2004. Biological effects of ultrafine model particles in human macrophages and epithelial cells in mono- and co-culture. Int J Hyg Environ Health. 207(4):353–361. [PubMed: 15471099]

Yang Q, Chen Y, Shi Y, Burnett RT, McGrail KM, Krewski D. 2003. Association between ozone and respiratory admissions among children and the elderly in vancouver, canada. Inhal Toxicol. 15(13):1297–1308. [PubMed: 14569494]

Zhang R, Dai Y, Zhang X, Niu Y, Meng T, Li Y, Duan H, Bin P, Ye M, Jia X et al. 2014. Reduced pulmonary function and increased pro-inflammatory cytokines in nanoscale carbon black-exposed workers. Part Fibre Toxicol. 11:73. [PubMed: 25497989]

Zheng R, Tao L, Jian H, Chang Y, Cheng Y, Feng Y, Zhang H. 2018. Nlrp3 inflammasome activation and lung fibrosis caused by airborne fine particulate matter. Ecotoxicol Environ Saf. 163:612–619. [PubMed: 30092543]

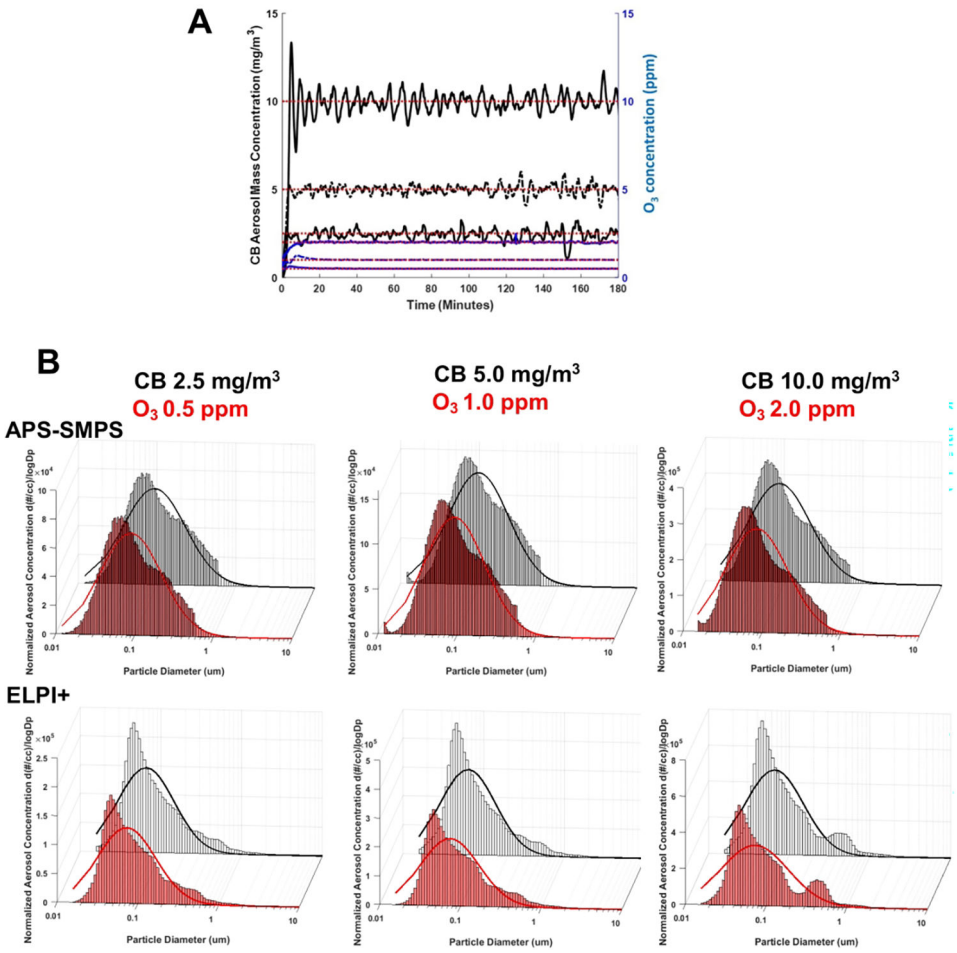

Figure 1. Aerosol exposure and characterization.

A) Real-time monitoring of CB and O_3 levels during different exposures. B) Aerosol size distribution of CB (2.5 mg/m^3, 5.0 mg/m^3 and 10.0 mg/m^3) and CB+O_3 (2.5 mg/m^3 + 0.5 ppm, 5.0 mg/m^3 + 1.0 ppm, 10.0 mg/m^3 + 2.0 ppm) aerosol particles collected from the inhalation exposure chamber using an aerosol particle sizer (APS) in combination with scanning mobility particle sizer (SMPS) and an electrical Low-Pressure Impactor (ELPI+).

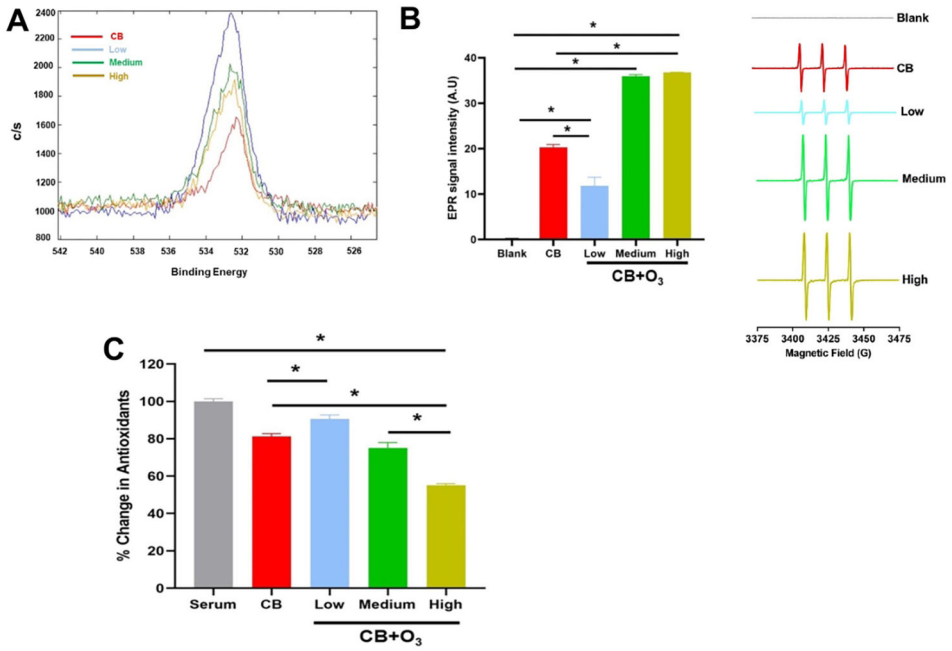

Figure 2. Acellular Characterization of aerosol reactivity.

A) XPS analysis representing surface oxygen contents of CB and CB+O_3 particles at low (2.5 mg/m^3 + 0.5 ppm), medium (5 mg/m^3 + 1 ppm) and high (10 mg/m^3 + 2 ppm) dose. B) Representative X-band Electron paramagnetic resonance (EPR) spectra of CM• in PBS with single (CB) and co-exposure (CB+O_3) particles suspension (50 μg/mL) at low (2.5 mg/m^3 + 0.5 ppm), medium (5 mg/m^3 + 1 ppm) and high (10 mg/m^3 + 2 ppm) dose. Histogram represents intensity of the first peak of EPR signals. C) FRAS assay of single (CB) and co-exposure (CB+O_3) aerosol at low (2.5 mg/m^3 + 0.5 ppm), medium (5 mg/m^3 + 1 ppm) and high (10 mg/m^3 + 2 ppm) exposure dose. Data are presented as mean ± standard error of mean of three independent experiments. Data analyzed by One-way ANOVA followed by Tukey's post-hoc test. *$p < 0.05$.

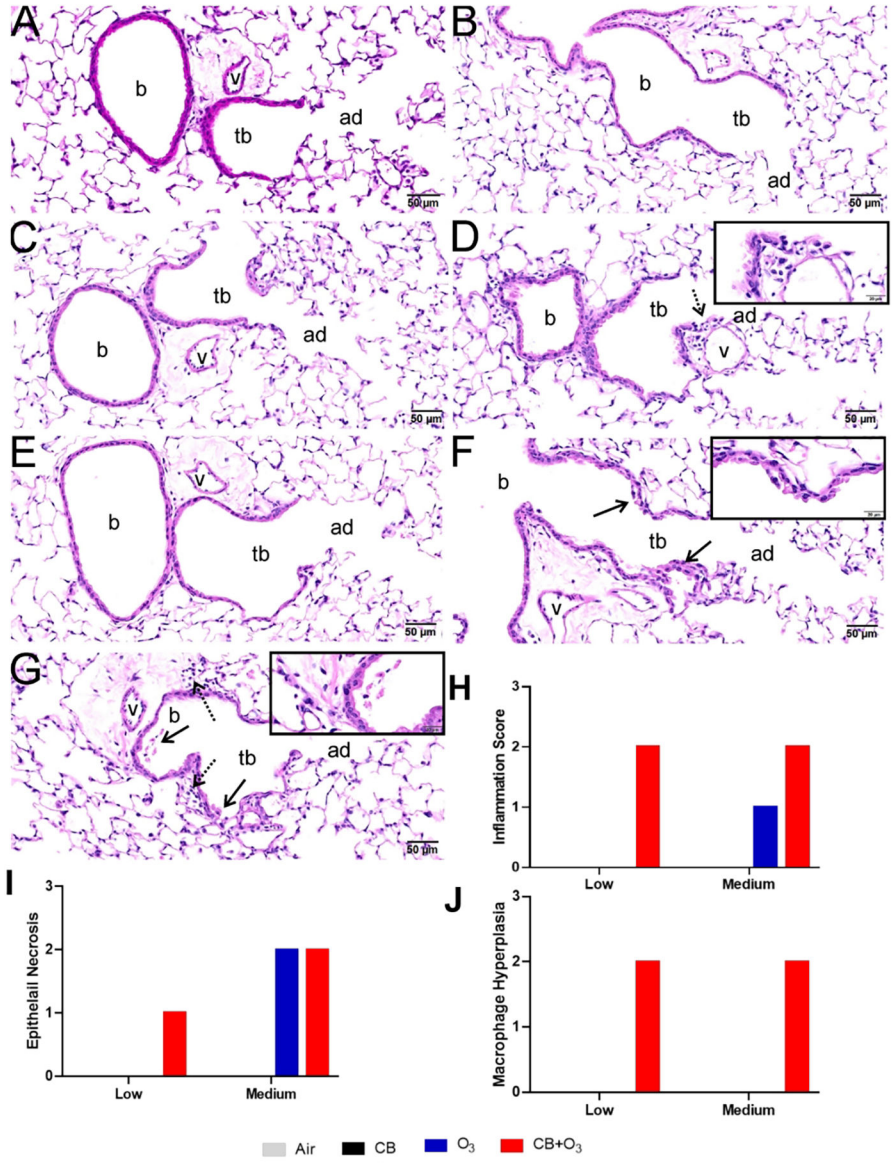

Figure 3. Histopathological assessments of lung tissue after low and medium dose exposures.

Lung tissues were collected 24 hours post-exposure, fixed in neutral buffered formalin, and stained with H&E. Light photomicrographs of sections from A) filtered air, B) CB 2.5 mg/m^3, C) O_3 0.5 ppm D) CB +O_3 (2.5 mg/m^3 + 0.5 ppm) and E) CB 5.0 mg/m^3, F) O_3 1.0 ppm G) CB +O_3 (5.0 mg/m^3 + 1.0 ppm). Tissues were semi-quantitatively scored in a blinded manner by a board-certified veterinary pathologist for H) inflammatory cell influx, I) airway epithelial injury/cell death and J) macrophage hyperplasia. b, bronchiole; tb, terminal bronchiole; ad, alveolar duct; v, blood vessel; stippled arrows, inflammatory cell infiltration; solid arrows, necrotic/exfoliated airway epithelial cells. Insets on panels D, F and G are higher magnification on the areas where pathological lesions are noted.

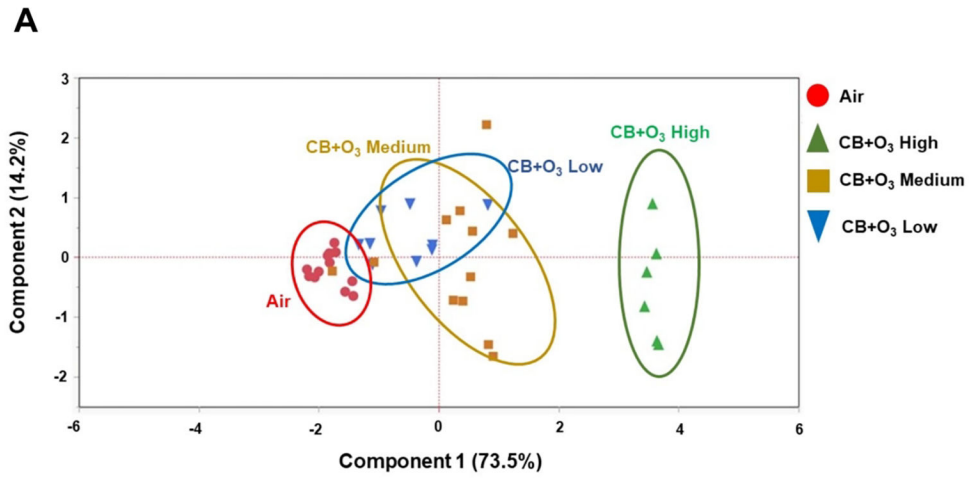

Figure 4. Score plot of the first two components of the principal component analysis showing pulmonary injury and inflammatory response

after exposure to air (control), CB, O_3 and CB+O_3 at low (2.5 mg/m^3 and/or 0.5 ppm), medium (5 mg/m^3 and/or 1 ppm) and high (10 mg/m^3 and/or 2ppm), for 3 hours followed by euthanasia 24 hours post exposure. The response of animals from each group and their clustering was highlighted qualitatively by the oval.

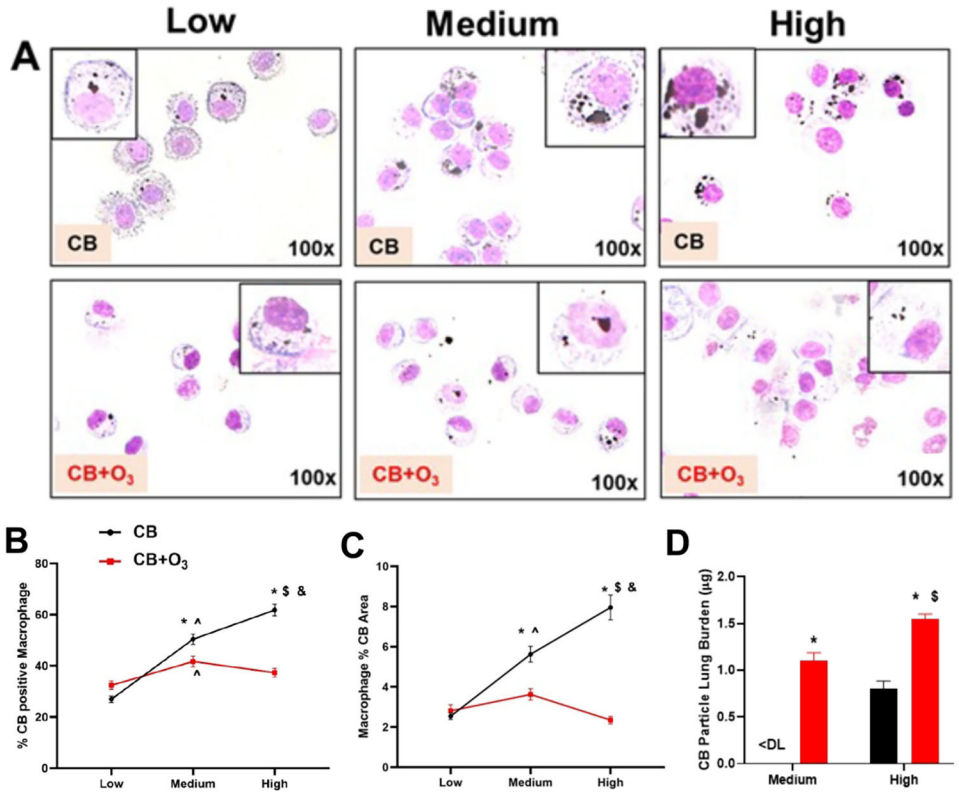

Figure 5. Particle uptake.

A) Representative images of *in-vivo* uptake of particles (CB and CB+O_3) by broncho-alveolar lavage macrophages (40X and 100X magnification) at low (0.5 ppm and/or 2.5 mg/m^3), medium (1 ppm and/or 5 mg/m^3) and high (2 ppm and/or 10 mg/m^3) exposures for 3 hours, followed by euthanasia 24 hours post exposure. Quantification of particle uptake by B) percentage particle positive macrophages, and C) percentage of particle area in macrophages. C) Lung burden quantification of particles (CB and CB+O_3) 24 hours post exposure. Data analyzed by two-way ANOVA followed by Tukey's post-hoc test. *$p < 0.05$ vs CB+O_3 at same dose, ^$p \leq 0.05$ low vs medium dose, \$$p \leq 0.05$ medium vs high dose, &$p < 0.05$ low vs high dose. <DL denotes lower than detection limit of the assay (0.8 µg/mL).

A

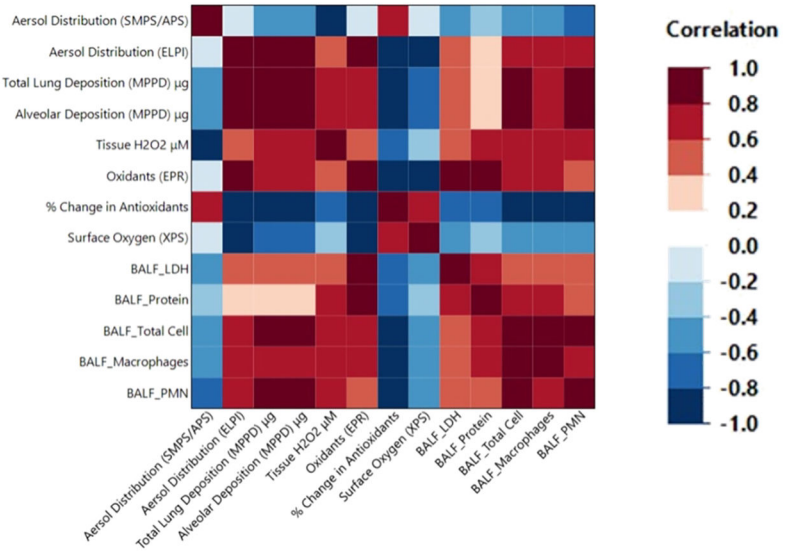

B

Characteristics		Top Correlated Variable	Pearson Correlations (Confidence Interval)
Aerosol Characteristics	Aerosol Size Distribution (ELPI)	Total and Alveolar Deposition	0.882 (0.756 – 0.945)
		BALF Total Cells	0.712 (0.455 – 0.859)
		BALF PMN	0.679 (0.403 – 0.842)
	Total Lung Deposition (MPPD)	BALF PMN	0.899 (0.790 – 0.953)
		BALF Total Cells	0.859 (0.712 – 0.934)
		BALF Macrophages	0.757 (0.530 – 0.883)
		BALF LDH	0.598 (0.247 – 0.810)
	Alveolar Deposition (MPPD)	BALF PMN	0.899 (0.789 – 0.953)
		BALF Total Cells	0.859 (0.712 – 0.934)
		BALF Macrophages	0.757 (0.530 – 0.883)
Oxidative Characteristics	% Change in Antioxidants (FRAS)	BALF Total Cells	-0.901 (-0.958 – -0.778)
		BALF Macrophage	-0.869 (-0.943 – -0.712)
		BALF PMN	-0.869 (-0.943 – -0.712)
	Oxidants (EPR)	BALF Protein	0.893 (0.634 – 0.972)
		BALF LDH	0.823 (0.442 – 0.952)
		Surface Oxygen	-0.989 (-0.998 – -0.938)
	Surface Oxygen (XPS)	BALF Total Cell	-0.587 (-0.790 – -0.266)
		BALF Macrophages	-0.574 (-0.738 – -0.248)
		BALF LDH	-0.421 (-0.710 – -0.011)

Figure 6. Multivariate analysis linking aerosol characteristics and oxidative properties of the mixtures to pulmonary injury and inflammation.

A) Heat map representing Pearson correlations of aerosol characteristics and oxidative characteristics of the mixtures with biological outcomes B) Table outlining the top correlated biological variables with aerosol characteristics and oxidative characteristics based on p-value.

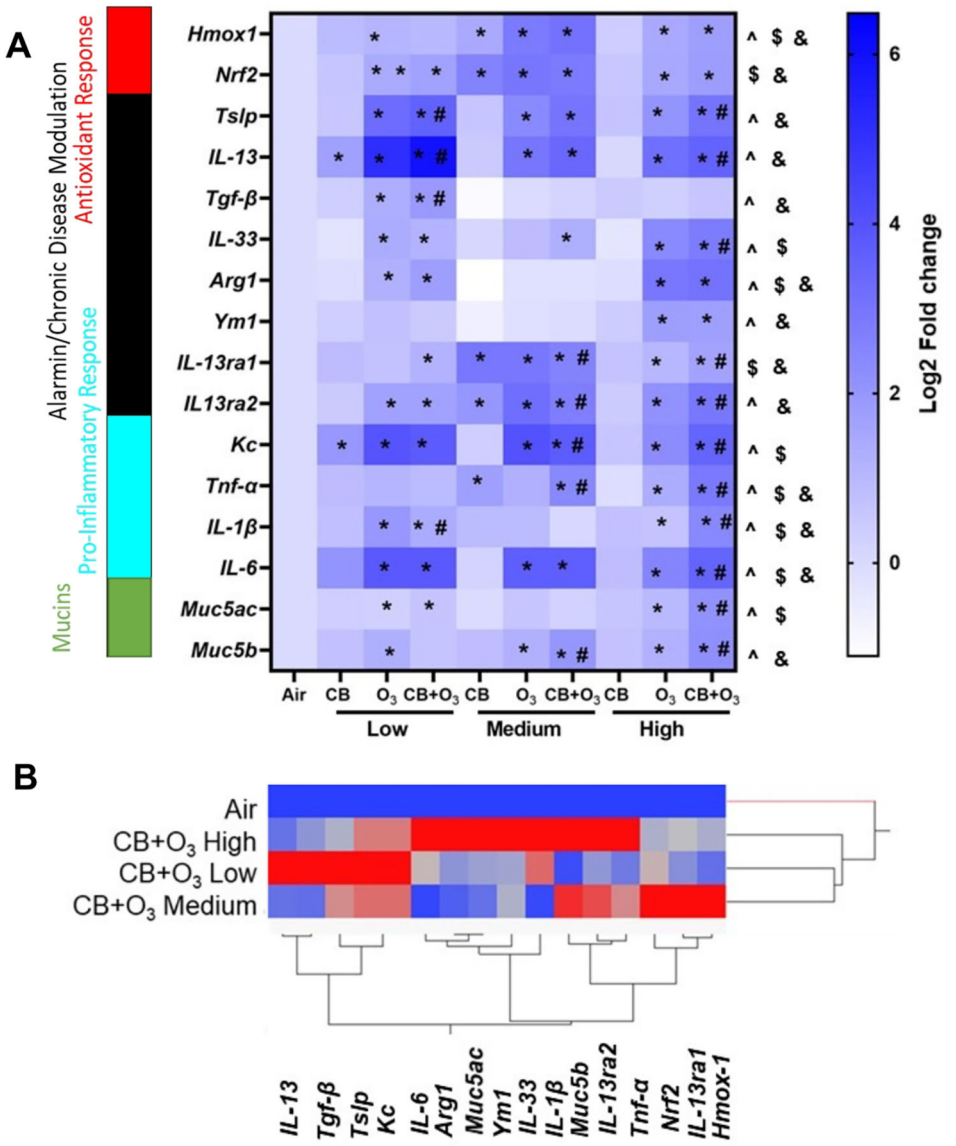

Figure 7. Lung tissue real-time mRNA expression.

A) Heat Map representing the fold changes of mRNA gene expression in lung tissue after exposure to air (control), CB, O_3 and CB+O_3 at low (2.5 mg/m^3 and/or 0.5 ppm), medium (5.0 mg/m^3 and/or 1 ppm) and high (10.0 mg/m^3 and/or 2.0 ppm), for 3 hours, followed by euthanasia 24 hours post exposure. The values are normalized to Log2 fold change. Data analyzed by Two-way ANOVA followed by Tukey's post-hoc test. *$p < 0.05$ vs control, #$p \leq 0.05$ vs CB+O_3 single exposure at same dose, ^$p \leq 0.05$ CB+O_3 low vs high dose, \$$p \leq 0.05$ CB+O_3 medium vs high dose, &$p \leq 0.05$ CB+O_3 low vs medium dose. B) Hierarchical Clustering Analysis (HCA) of mRNA gene expression after exposure to air (control) and CB+O_3 at low (2.5 mg/m^3 + 0.5 ppm), medium (5.0 mg/m^3 + 1.0 ppm) and high (10.0 mg/m^3 + 2.0 ppm) doses, for 3 hours, followed by euthanasia 24 hours post exposure.

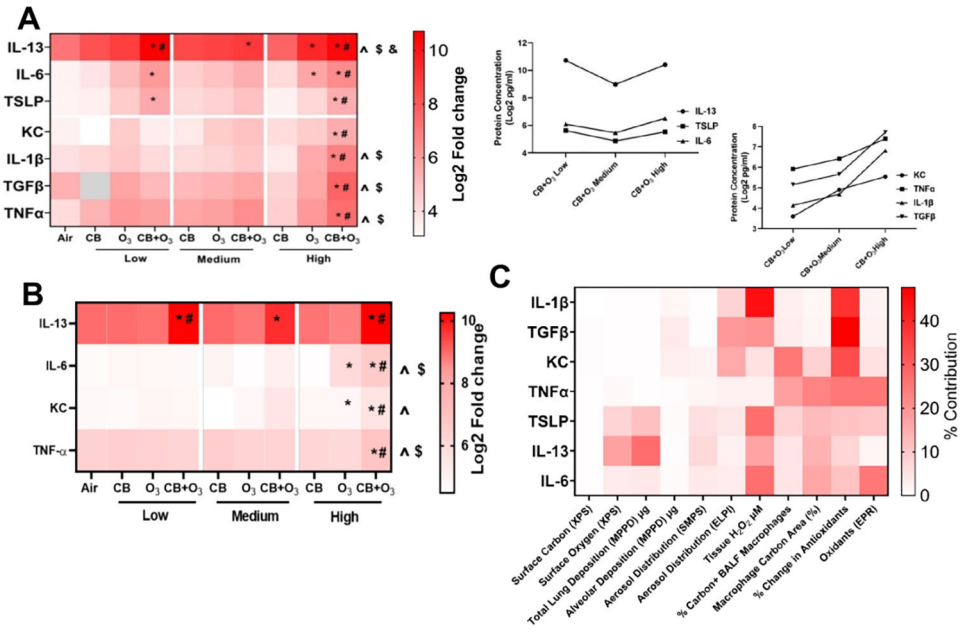

Figure 8. Predictor screening of broncho-alveolar lavage cytokines.

A) Heat Map representing the cytokine quantification in broncho-alveolar lavage fluid after exposure to air (control), CB, O_3 and CB+O_3 at low (2.5 mg/m^3 and/or 0.5 ppm), medium (5.0 mg/m^3 and/or 1.0 ppm) and high (10.0 mg/m^3 and/or 2.0 ppm) doses for 3 hours followed by euthanasia 24 hours post exposure. B) Heat Map representing the cytokine quantification in lung tissue homogenate after exposure to air (control), CB, O_3 and CB+O_3 at low (2.5 mg/m^3 and/or 0.5 ppm), medium (5.0 mg/m^3 and/or 1.0 ppm) and high (10.0 mg/m^3 and/or 2.0 ppm) doses for 3 hours followed by euthanasia 24 hours post exposure The values are normalized to Log2 fold change. Data analyzed by two-way ANOVA followed by Tukey's post-hoc test. *$p < 0.05$ vs control, #$p \leq 0.05$ CB+O_3 vs single exposure at same dose, ^$p \leq 0.05$ CB+O_3 low vs high dose, \$$p \leq 0.05$ CB+O_3 medium vs high dose, &$p \leq 0.05$ CB+O_3 low vs medium dose. C) Heat map representing percentage contribution of aerosol characteristics in cytokine production based on boot strap forest approach.

Table 1.

Exposure Design for the study.

	Treatment	Target Concentration
Low	Carbon Black	2.5 mg/m^3
	Ozone	0.5 ppm
	Carbon Black + Ozone	2.5 mg/m^3 + 0.5 ppm
Medium	Carbon Black	5 mg/m^3
	Ozone	1 ppm
	Carbon Black + Ozone	5 mg/m^3 + 1 ppm
High	Carbon Black	10 mg/m^3
	Ozone	2 ppm
	Carbon Black + Ozone	10 mg/m^3 + 2 ppm

Target exposure concentration for low, medium, and high dose of carbon black (CB), ozone (O_3) and carbon black + ozone ($CB+O_3$)

Table 2.

Aerosol distributions and deposition calculations.

	SMPS/APS CMD nm (GSD)	SMPS/APS #/cc	ELPI+ CMD nm (GSD)	ELPI+ #/cc	Alveolar Deposited Dose (μg) (MPPD)	Total Deposited Dose (μg) (MPPD)
CB 2.5 mg/m^3	92.3 (2.47)	0.66E+05	64.8 (2.23)	1.27E+05	1.17	2.33
CB 2.5 mg/m^3 + O_3 0.5 ppm	89.7 (2.46)	0.70E+05	72.6 (2.29)	1.19E+05	1.23	2.42
CB 5.0 mg/m^3	97.1 (2.42)	1.20E+05	63.6 (2.19)	2.54E+05	2.46	4.87
CB 5.0 mg/m^3 + O_3 1.0 ppm	93.0 (2.44)	1.28E+05	73.9 (2.31)	2.13E+05	2.47	4.87
CB 10.0 mg/m^3	85.8 (2.48)	2.72E+05	65.2 (2.28)	4.22E+05	4.92	9.68
CB 10.0 mg/m^3 + O_3 2.0 ppm	85.7 (2.49)	2.89E+05	72.5 (2.59)	3.48E+05	4.82	9.54

Count median diameters (CMD) and geometric standard deviations (GSD) calculations at the indicated exposure concentrations from CB and CB+O_3 using SMPS/APS and ELPI+. Total lung and alveolar deposition estimates using Multiple Path Particle Dosimetry (MPPD) software at the end of exposure without accounting for clearance.

Table 3.

Pulmonary injury and inflammation.

	BALF Total Cell (X10^5)	BALF Macrophages (× 10^5)	BALF PMN (X 10^5)	BALF LDH (Fold change to Air)	BALF Total Protein (mg/mL)	Tissue H_2O_2 (nM)	Serum H_2O_2 (μM)	Serum Oxidants EPR (arb. units)	Respiratory Resistance ($cmH_2O.s/mL$)	Dynamic Compliance (mL/cmH_2O)	Forced Expiratory Volume (0.1) (mL)
Air	6.1 ± 1.9	6.1 ± 1.9	0 ± 0	1.00 ± 0.3	87.5 ± 22.7	57.3 ± 15.5	1.08±0.19	2.91±0.41	0.6 ± 0.11	0.037 ± 0.001	1.0 ± 0.06
CB Low	6.4 ± 0.8	6.4 ± 0.8	0 ± 0	2.84 ± 0.9	116.6 ± 25.4	61.6 ± 13.6	1.46±0.22	2.94±0.49	0.6 ± 0.01	0.032 ± 0.004	0.93 ± 0.03
CB Med	5.8 ± 1.8	5.8 ± 1.8	0 ± 0	1.19 ± 0.1	83.9 ± 17.7	93.7 ± 36.5	1.69±0.13	2.62±1.53	0.6 ± 0.03	0.037 ± 0.004	0.89 ±0.11
CB High	6.3 ± 1.5	6.3 ± 1.5	0 ± 0	0.50 ± 0.1	82.02 ± 10.0	75.2 ± 41.2	1.38±0.75	2.13±0.77	0.7± 0.08	0.035 ± 0.001	0.92 ± 0.02
O_3 Low	9.2 ± 4.3	9.1 ± 4.3	0.1 ± 0.1	1.58 ± 0.7	228.4 ± 49.2 *	66.7 ± 16.7	1.68±0.19 *	2.91±0.40 *	0.6 ± 0.02	0.034 ± 0.003	0.94 ± 0.03
O_3 Med	9.1 ± 2.6	8.8 ± 2.6	0.3 ± 0.1	2.44 ± 2.0	211 ± 41.9 *	57.9 ± 36.2	1.22±0.25	2.23±1.17	0.7± 0.09	0.033 ± 0.002	0.95 ± 0.01
O_3 High	18.3 ± 3.1	16.5 ± 2.8 *	1.8 ± 0.4 *	1.78 ± 0.2 *	232.4 ± 35.8 *	88.7 ± 25.8	1.60±0.15 *	2.34±0.26	0.8 ± 0.11	0.033 ± 0.002	0.93 ± 0.04
CB+O_3 Low	10.6 ± 3.4	10.5 ± 3.5	0.1 ± 0.1	1.57 ± 0.7	237 ± 93.9 *	85.7 ± 14.4	1.73±0.10 *	2.28±0.11	0.6 ± 0.03	0.037 ± 0.001	0.95 ± 0.03
CB+O_3 Med	15.4 ± 4.9	14.7 ± 4.5	0.7 ± 0.6	1.50 ± 1.0	268 ± 143 *	51.3 ± 3	1.50±0.15	2.43±0.50	0.7 ± 0.06 *	0.032 ± 0.002 *	0.82 ± 0.05
CB+O_3 High	25.0 ± 1.4 *#^$	22.0 ± 1.9 *#^$	3.0 ± 0.7 *#^$	3.80 ± 1.0 *#^$	341.4 ± 42.6 *#	207.1 ± 60.5 *#^$	2.29±0.19 *#	4.98±0.55 *#	0.8 ± 0.07 *	0.030 ± 0.001 *	0.85 ±0.06 *

Bronchoalveolar lavage total cell, macrophages, neutrophils/pmn, LDH, total protein and tissue hydrogen peroxide concentration after exposure to air (control), CB, O_3 and CB+O_3 at low (2.5 mg/m^3 and/or 0.5 ppm), medium (5.0 mg/m^3 and/or 1.0 ppm) and high (10.0 mg/m^3 and/or 2.0 ppm) 3 hours, followed by euthanasia 24 hours post exposure. Data are presented as mean ± standard deviation. n = 5–8 mice per group. Data analyzed by One-way ANOVA followed by Tukey's post-hoc test.

* $p \leq 0.05$ vs control

$p \leq 0.05$ CB+O_3 vs single exposure at same dose

^ $p \leq 0.05$ CB+O_3 low vs high dose

$ $p < 0.05$ CB+O_3 medium vs high dose.

Table 4.

BMD modeling of lung injury (BALF LDH and BALF total protein) and lung inflammation (total cell influx and alveolar macrophages) parameters after exposure to air (control), CB, O_3 and CB+O_3 for 3 hours followed by euthanasia 24 hours post exposure.

Exposure	BALF LDH		BALF Total Protein		Total Cell Influx		Alveolar Macrophages	
	BMD	BMDL	BMD	BMDL	BMD	BMDL	BMD	BMDL
CB (mg/m^3)	9.39	7.26	12.06	8.40	42.76	9.39	42.80	9.40
O_3 (ppm)	2.39	1.46	0.84	0.60	0.90	0.56	0.93	0.66
CB+O_3 (mg/m^3 + ppm)	4.19+0.84	3.5+0.71	3.7+0.74	2.7+0.55	1.96+0.39	1.43+0.29	3.4+0.68	2.9+0.58